

CRNL/TM-11202

orml

OAK RIDGE
NATIONAL
LABORATORY

MARTIN MARIETTA

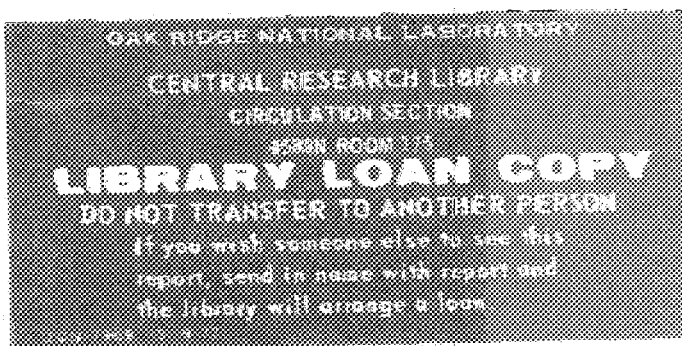
MARTIN MARIETTA ENERGY SYSTEMS LIBRARIES



3 4456 0348596 7

Electron-Impact Ionization Data
for the Nickel Isonuclear Sequence

M. S. Pindzola
D. C. Griffin
C. Bottcher
M. J. Buie
D. C. Gregory



OPERATED BY
MARTIN MARIETTA ENERGY SYSTEMS, INC.
FOR THE UNITED STATES
DEPARTMENT OF ENERGY

This report has been reproduced directly from the best available copy.

Available to DOE and DOE contractors from the Office of Scientific and Technical Information, P.O. Box 62, Oak Ridge, TN 37831; prices available from (615) 576-8401, FTS 626-8401.

Available to the public from the National Technical Information Service, U.S. Department of Commerce, 5285 Port Royal Rd., Springfield, VA 22161.

NTIS price codes—Printed Copy: A04 Microfiche A01

This report was prepared as an account of work sponsored by an agency of the United States Government. Neither the United States Government nor any agency thereof, nor any of their employees, makes any warranty, express or implied, or assumes any legal liability or responsibility for the accuracy, completeness, or usefulness of any information, apparatus, product, or process disclosed, or represents that its use would not infringe privately owned rights. Reference herein to any specific commercial product, process, or service by trade name, trademark, manufacturer, or otherwise, does not necessarily constitute or imply its endorsement, recommendation, or favoring by the United States Government or any agency thereof. The views and opinions of authors expressed herein do not necessarily state or reflect those of the United States Government or any agency thereof.

ORNL/TM-11202

Physics Division

**ELECTRON-IMPACT IONIZATION DATA
FOR THE NICKEL ISONUCLEAR SEQUENCE**

M. S. Pindzola, D. C. Griffin, C. Bottcher,
M. J. Buie, and D. C. Gregory

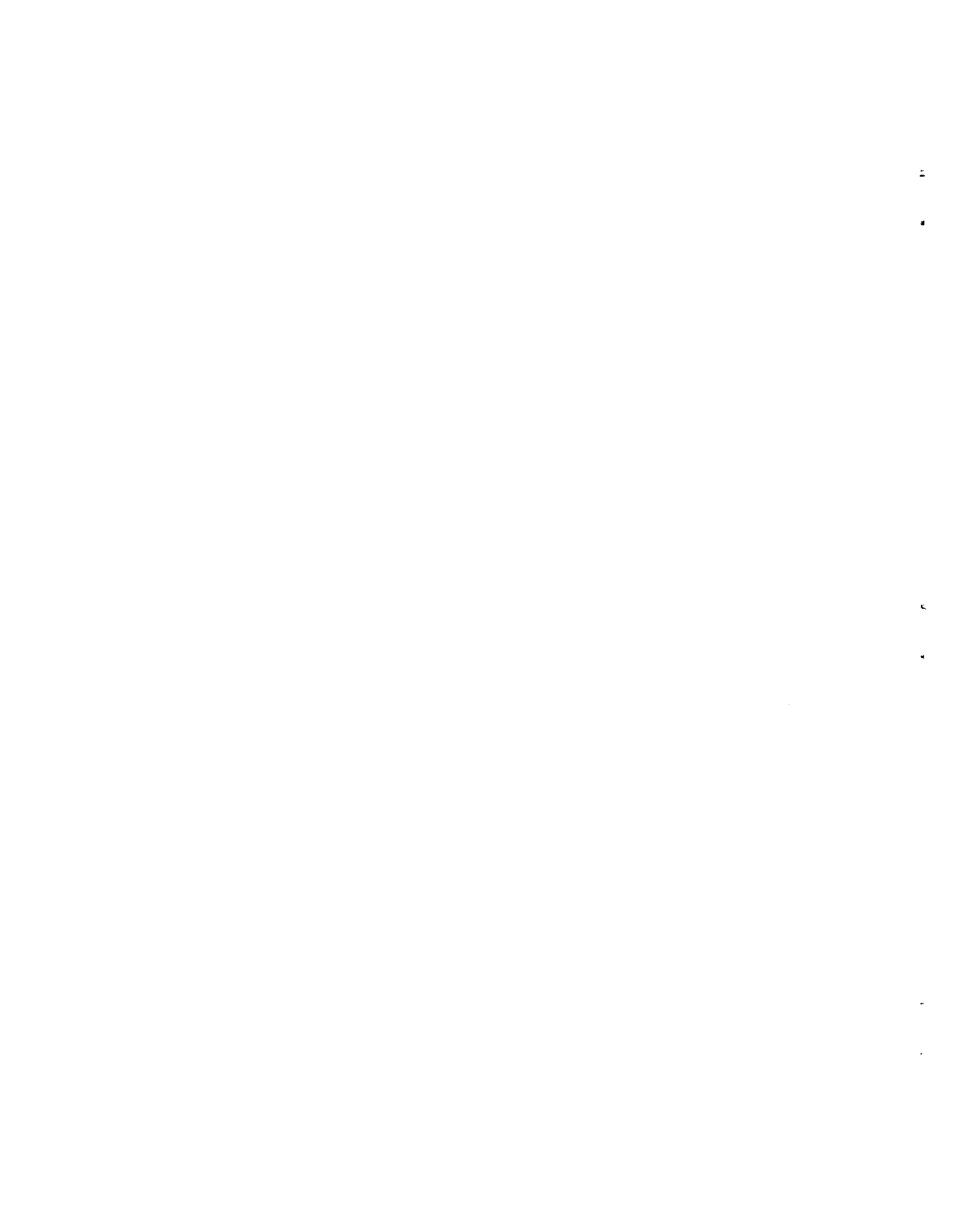
Date Published - March 1990

Prepared for the
Office of Fusion Energy
U.S. Department of Energy
Washington, D.C. 20545
Budget Activity No. AT 05 20 26 0

Prepared by the
OAK RIDGE NATIONAL LABORATORY
Oak Ridge, Tennessee 37831
Operated by
MARTIN MARIETTA ENERGY SYSTEMS, INC.
for the
U.S. DEPARTMENT OF ENERGY
under Contract DE-AC05-84OR21400



3 4456 0348596 7



CONTENTS

	<u>Page</u>
ABSTRACT	1
1. INTRODUCTION	1
2. THEORETICAL METHODS	3
3. CROSS SECTIONS FOR Ni ATOMIC IONS	5
3.1 Ni ⁺ Results	5
3.2 Ni ²⁺ Results	5
3.3 Ni ³⁺ Results	5
3.4 Ni ⁴⁺ Results	6
3.5 Ni ⁵⁺ Results	6
3.6 Ni ⁶⁺ Results	7
3.7 Ni ⁷⁺ Results	7
3.8 Ni ⁸⁺ Results	7
3.9 Ni ⁹⁺ Results	8
3.10 Ni ¹⁰⁺ Results	8
3.11 Ni ¹¹⁺ Results	8
3.12 Ni ¹²⁺ Results	9
3.13 Ni ¹³⁺ Results	9
3.14 Ni ¹⁴⁺ Results	10
3.15 Ni ¹⁵⁺ Results	10
3.16 Ni ¹⁶⁺ Results	11
3.17 Ni ¹⁷⁺ Results	11
3.18 Ni ¹⁸⁺ through Ni ²⁶⁺ Results	11
4. RATE COEFFICIENTS FOR Ni ATOMIC IONS	12
ACKNOWLEDGMENTS	13
REFERENCES	13

ELECTRON-IMPACT IONIZATION DATA FOR THE NICKEL ISONUCLEAR SEQUENCE

M. S. Pindzola,^a D. C. Griffin,^b C. Bottcher,
M. J. Buie,^c and D. C. Gregory

ABSTRACT

Atomic data for the electron impact ionization of ions in the nickel isonuclear sequence are reviewed. In 8 of the 28 ions of the nickel isonuclear sequence, experiment and theory are compared. In many of the ions, excitation-autoionization contributions to the total cross section are found to be quite important. For intermediate charge state ions a large fraction of the experimental cross section may be attributed to ionization from metastable levels of low-lying excited configurations. Maxwellian collisional rate coefficients are calculated from the cross section data and presented in tabular, graphical, and parametrized form.

1. INTRODUCTION

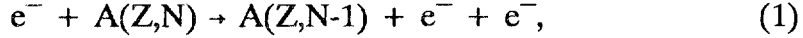
The principal ionization mechanism found in plasma transport modeling of impurities in magnetic fusion experiments is electron-impact ionization. Accurate ionization rate coefficients are thus needed for many transition series metals, due to their presence in containment vessels. Recently a joint theoretical and experimental research project to study the electron-impact ionization of atomic ions along the entire Fe isonuclear sequence was completed.¹⁻⁴ In this report we present the results of similar calculations and measurements for electron ionization of atomic ions in the Ni isonuclear sequence.

A number of collisional processes can contribute to the total electron-impact ionization of atomic ions. In addition to direct ionization from an initial ion with atomic number A and N bound electrons:

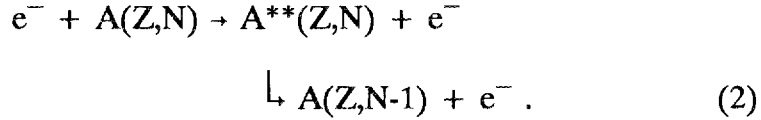
^aDepartment of Physics, Auburn University, Auburn, AL 36849.

^bDepartment of Physics, Rollins College, Winter Park, FL 32789.

^cDepartment of Physics, Auburn University, Auburn, AL 36849; present address, Naval Research Lab./code 4720, 4555 Overlook Ave. SW, Washington, DC 20375.

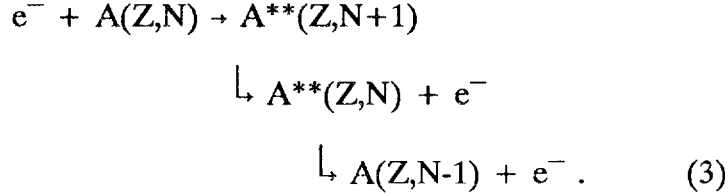


we can have inner-shell excitation followed by autoionization:



Studies over the past decade⁵ have shown that the contributions of excitation autoionization can dominate the total ionization cross section for ions in relatively low stages of ionization, when the doubly excited states resulting from $\Delta n=0$ inner-shell excitations are autoionizing. However, inner-shell excitations involving $\Delta n \geq 1$ excitations can also make significant contributions to the total ionization cross section, especially in higher stages of ionization. For a given isonuclear sequence, direct ionization cross sections decrease rather rapidly with ionization stage, while the magnitude of the $\Delta n \geq 1$ excitation cross sections tend to gradually increase; this, of course, results in a significant increase in the relative magnitude of the indirect contributions.

In addition to the ionization processes described in Eqs. (1) and (2), we can also have contributions from resonant recombination followed by double autoionization:



In order to determine whether this last process will contribute to the total ionization cross section, one must first determine the relative probability of sequential autoionization from the doubly excited state of the $(N+1)$ -electron ion to all possible states of the $(N-1)$ -electron ion versus the probability of all possible autoionizing and (or) radiative transitions to bound states of the $(N+1)$ - or N -electron ions. In a complex ion, this typically involves many hundreds of transitions for a given $(N+1)$ -electron level. For this reason this process is not well understood. As we shall see, comparisons of calculations which include only processes (1) and (2) with experimental cross sections indicate that this process does make contributions to the total ionization of several of the ions considered here.

In addition to ionization from the ground states of atomic ions, it is important to consider ionization from possible metastable states which might be heavily populated in a given plasma. One might expect that ionization from low-lying excited configurations to be important when the number of long-lived excited states (those that are forbidden to decay to the ground state because of J selection rules) is large in comparison to the number of relatively short-lived excited states plus the total number of states within the ground configuration. Thus when performing purely theoretical studies, we have normally included ionization from such low-lying excited configurations only when the ratio of metastable states to all states in the excited configuration and ground configuration is relatively large. However, extensive comparisons of theoretical calculations with cross section measurements in which the ECR ion source at Oak Ridge National Laboratory was employed indicate that this ion source preferentially populates some of the low-lying, long-lived states. Whether this is true in other laboratory and astrophysical plasmas is still an unanswered question.

The remainder of this report is arranged as follows. In the next section we briefly summarize the theoretical and calculational methods employed to determine the ionization cross section. In Sect. 3, we discuss the results of our cross section calculations for the Ni ions and compare them with available experimental data. Finally in Sect. 4, Maxwellian collisional rate coefficients are calculated from the cross section data and presented in tabular, graphical, and parametrized form.

2. THEORETICAL METHODS

The total single ionization cross section, ignoring interference effects between the direct ionization and excitation-autoionization processes, may be written as:

$$\sigma_{\text{tot}}(i) = \sum_f \sigma_{\text{ion}}(i \rightarrow f) + \sum_j \sigma_{\text{exc}}(i \rightarrow j) B_j^a , \quad (4)$$

where $\sigma_{\text{ion}}(i \rightarrow f)$ is the direct ionization cross section from the initial configuration to a particular level f within the ionized configurations and $\sigma_{\text{exc}}(i \rightarrow j)$ is the excitation cross section from the initial configuration to a particular level j within the core-excited configurations. The branching ratio for autoionization, B_j^a , from level j is given by:

$$B_j^a = \frac{\sum_m A_a(j \rightarrow m)}{\sum_m A_a(j \rightarrow m) + \sum_n A_f(j \rightarrow n)} , \quad (5)$$

where $A_a(j \rightarrow m)$ is the autoionizing rate from level j and $A_r(j \rightarrow n)$ is the radiative rate from level j . The further indirect ionization process of resonant-recombination double autoionization is not included in the calculations.

The direct ionization contributions, given by the first term of Eq. (4), may be obtained using distorted-wave methods.⁶⁻⁸ For the atomic ion of interest, a configuration-average collision cross section, $\bar{\sigma}_{\text{ion}}(n\ell)$, is calculated for each ionized subshell of the initial configuration which may contribute to single ionization. Cross sections for the other two or three subshells are needed for a typical nickel ion. The configuration-average cross sections, $\bar{\sigma}_{\text{ion}}(n\ell)$, are then statistically partitioned over all levels of the final ionized configurations. Finally the direct ionization cross sections are summed taking explicit account of the energy position of each ionized level calculated using the atomic structure package of Cowan.⁹

For ease in accessing the results of the numerical calculations, the direct ionization cross section for each subshell may be written in the following parameterized form:

$$\bar{\sigma}_{\text{ion}}(n\ell) = \frac{1}{IE} \left[A \left(1 - \frac{I}{E} \right) + B \left(1 - \frac{I}{E} \right)^2 + C \ell n \left(\frac{E}{I} \right) + D \frac{I}{E} \ell n \left(\frac{E}{I} \right) \right], \quad (6)$$

where E is the incident electron energy in eV, I is the subshell ionization potential in eV, and the cross section is in cm². The parameters A , B , C , and D for the ground and certain excited configurations of all Ni ions are presented in Table 1.

The excitation-autoionization contributions, given by the second term of Eq. (4), may be obtained using distorted-wave methods.¹⁰⁻¹¹ For many atomic ions of interest, a configuration-average collision cross section, $\bar{\sigma}_{\text{exc}}(n\ell \rightarrow n'\ell')$, is calculated for each subshell excitation of the initial configuration which may contribute to single ionization. Cross sections for up to 40 excitations are needed for a typical nickel ion. The configuration-average cross sections, $\bar{\sigma}_{\text{exc}}(n\ell \rightarrow n'\ell')$, are then statistically partitioned over all levels of the final core-excited configurations. Finally the excitation cross sections are summed taking explicit account of both the energy position and branching ratio of each core-excited level calculated using the atomic structure package of Cowan.⁹ This method is a reasonable approximation when most of the levels within the final core-excited configuration are above the ionization limit, the branching ratios B_j^a are all close to one, and correlation in the initial and final states is small.

For certain atomic ions of interest, a level-to-level collision cross section, $\sigma_{\text{exc}}(i \rightarrow j)$, is calculated for transitions to each and every level of the final core-excited configurations. The excitation cross sections are then summed in the same

manner as the configuration-average method. The method is able to handle those cases where only a few levels are above the ionization limit and where branching ratios B_i^a are not close to one. In addition, correlation effects are easily incorporated into a level-to-level distorted-wave method. The major drawback of the method is that a full level-to-level cross section calculation for a single subshell excitation may take a couple of orders of magnitude more CPU time than the corresponding configuration-average calculation. The increase in time scales roughly as the average number of levels per final core-excited configuration. A worst case example is the $3p \rightarrow 4f$ excitation for the ground configuration of Ni^{5+} , resulting in a $3s^2 3p^5 3d^5 4f$ configuration with 2382 levels.

3. CROSS SECTIONS FOR Ni ATOMIC IONS

3.1 Ni^+ Results

In Fig. 1 the crossed-beams measurements of Montague and Harrison¹² for Ni^+ are compared with a configuration-average distorted-wave calculation for the $3s^2 3p^6 3d^9$ ground configuration. The calculation only includes direct ionization of the 3d subshell. Theory clearly overestimates the cross section in the threshold energy region.

3.2 Ni^{2+} Results

In Fig. 2 a configuration-average distorted-wave calculation for the $3s^2 3p^6 3d^8$ ground configuration of Ni^{2+} is presented. The calculation includes the $3p \rightarrow 3d$ excitation and direct ionization of the 3d subshell.

In Fig. 3 the configuration-average distorted-wave results are compared with the R-matrix LS close-coupling results of Burke, Fon, and Kingston.¹³ All 6 LS terms of the $3s^2 3p^5 3d^9$ configuration are included in the R-matrix calculation, while the distorted-wave calculation includes all 12 autoionizing levels. Reasonable agreement is found between the two calculations. The wavelike features in the R-matrix calculation are due to resonant-recombination followed by double autoionization. This additional indirect process is not included in the distorted-wave calculations.

3.3 Ni^{3+} Results

In Fig. 4 the crossed-beams measurements of Gregory and Howald¹⁴ for Ni^{3+} are compared with a configuration-average distorted-wave calculation for the

$3s^23p^63d^7$ ground configuration. The calculation includes the $3p \rightarrow 3d$ excitation and direct ionization of the 3d and 3p subshells. Almost half of the 3p direct ionization contributes to double ionization of Ni^{3+} , since 54 of the 110 levels of the $3s^23p^53d^7$ configuration are autoionizing. Theory clearly overestimates the cross section over much of the energy range.

In Fig. 5 experiment is compared with both the configuration-average distorted-wave results and the R-matrix LS close-coupling results of Burke, Fon, and Kingston.¹³ Only 6 of the 19 possible LS terms of the $3s^23p^53d^8$ configuration are included in the R-matrix calculation, while the distorted-wave calculation included all 45 autoionizing levels. The 6 LS terms included are expected, however, to contain the bulk of the $3p \rightarrow 3d$ excited collision strength. Reasonable agreement is found between the two calculations, although both overestimate the experimental cross section at the higher energies. The wave-like features in the R-matrix calculation are due to resonant-recombination processes.

3.4 Ni^{4+} Results

In Fig. 6 a configuration-average distorted-wave calculation for the $3s^23p^63d^6$ ground configuration of Ni^{4+} is presented. The calculation includes the $3p \rightarrow 3d$ excitation and direct ionization of the 3d and 3p subshells. The $3p \rightarrow 3d$ excitation is reduced significantly, since only 54 of the 110 levels of the $3s^23p^53d^7$ configuration are autoionizing.

3.5 Ni^{5+} Results

In Fig. 7 the crossed-beams measurements of Wang, Rinn, and Gregory¹⁵ for Ni^{5+} are compared with a configuration-average distorted-wave calculation for the $3s^23p^63d^5$ ground configuration. The calculation includes 41 excitations and direct ionization of the 3d, 3p, and 3s subshells. The largest excitations are $3p \rightarrow 4p$, in which 1190 of the 1208 levels of the $3s^23p^53d^54p$ configuration are autoionizing and $3s \rightarrow 3d$, in which all 63 levels of the $3s3p^63d^6$ configuration are autoionizing. Other important excitations are $3p \rightarrow 4d$, $3p \rightarrow 5p$, $3s \rightarrow 4s$, $3p \rightarrow 4s$, and $3p \rightarrow 4f$. The $3p \rightarrow 3d$ excitation is absent, since none of the 180 levels of the $3s^23p^53d^6$ configuration are autoionizing. An n^{-3} rule is used to estimate $3p \rightarrow n\ell$ and $3s \rightarrow n\ell$ excitation-autoionization contributions for $n \geq 9$. The agreement between theory and experiment is reasonable.

3.6 Ni⁶⁺ Results

In Fig. 8 the crossed-beams measurements of Wang, Rinn, and Gregory¹⁵ for Ni⁶⁺ are compared with a configuration-average distorted-wave calculation for the 3s²3p⁶3d⁴ ground configuration. The calculation includes 41 excitations and direct ionization of the 3d, 3p, and 3s subshells. The largest excitation is 3p → 4p, in which 450 of the 1038 levels of the 3s²3p⁵3d⁴4p configuration are autoionizing. Other important excitations are 3p → 5p, 3p → 4d, 3p → 4f, and 3s → 4s. The 3s → 3d excitation is greatly reduced, since only 6 of the 74 levels of the 3s3p⁶3d⁵ configuration are autoionizing. The n³ rule is used to estimate n≥9 excitation-autoionization contributions. The agreement between theory and experiment is quite reasonable from threshold to around 700 eV.

3.7 Ni⁷⁺ Results

In Fig. 9 the crossed-beams measurements of Wang, Rinn, and Gregory¹⁵ for Ni⁷⁺ are compared with a configuration-average distorted-wave calculation for the 3s²3p⁶3d³ ground configuration. The calculation includes 39 excitations and direct ionization of the 3d, 3p, and 3s subshells. The largest excitations are 3p → 4f, in which 1169 of the 1180 levels of the 3s²3p⁵3d³4f configuration are autoionizing and 3p → 5p, in which all 613 levels of the 3s²3p⁵3d⁵5p configuration are autoionizing. Other important excitations are 3s → 4s and 3p → 5f. The 3p → 4p excitation is greatly reduced, since only 44 of the 613 levels of the 3s²3p⁵3d³4p configuration are autoionizing. The n³ rule is used to estimate the n≥9 excitation-autoionization contributions. The agreement between theory and experiment is excellent from threshold to around 500 eV.

3.8 Ni⁸⁺ Results

In Fig. 10 the crossed-beams measurements of Wang, Rinn, and Gregory¹⁵ for Ni⁸⁺ are compared with a configuration-average distorted-wave calculation for the 3s²3p⁶3d² ground configuration. The calculation includes 38 excitations and direct ionization of the 3d, 3p, and 3s subshells. The largest excitations are 3p → 5p, in which 184 of the 256 levels of the 3s²3p⁵3d²5p configuration are autoionizing, and 3p → 5f in which all 472 levels of the 3s²3p⁵3d²5f configuration are autoionizing. Other important excitations are 3p → 6p and 3p → 6f. The n≥9 excitation-autoionization contributions for 3p → nℓ and 3s → nℓ, estimated by the n³ rule, increase the total cross section by about 8%. The agreement between theory and experiment is excellent from threshold to around 500 eV.

3.9 Ni⁹⁺ Results

In Fig. 11 a configuration-average distorted-wave calculation for the $3s^23p^63d$ ground configuration of Ni⁹⁺ is presented. The calculation includes 34 excitations and direct ionization of the 3d, 3p, and 3s subshells. The largest excitation is $3p \rightarrow 5f$ in which all 113 levels of the $3s^23p^53d5f$ configuration are autoionizing. Other important excitations are $3p \rightarrow 6p$, $3p \rightarrow 6f$, and $2p \rightarrow 3d$. The $n \geq 9$ excitation-autoionization contributions for $3p \rightarrow n\ell$ and $3s \rightarrow n\ell$, estimated by the n^3 rule, increase the total cross section by about 12%.

3.10 Ni¹⁰⁺ Results

In Fig. 12 a configuration-average distorted-wave calculation for the $3s^23p^6$ ground configuration of Ni¹⁰⁺ is presented. The calculation includes the $2p \rightarrow 3d$ and $2p \rightarrow 4\ell$ ($\ell = 0,1,2,3$) excitations and direct ionization of the 3p and 3s subshells.

In Fig. 13 a configuration-average distorted-wave calculation for the $3s^23p^53d$ excited configuration of Ni¹⁰⁺ is presented. The calculation includes the $3s \rightarrow 4d$, $3s \rightarrow 5\ell$ ($\ell = 0,1,2$), $2p \rightarrow 3p$, $2p \rightarrow 3d$, and $2p \rightarrow 4\ell$ ($\ell = 0,1,2,3$) excitations and direct ionization of the 3d, 3p, and 3s subshells. The largest excitation is $2p \rightarrow 3d$. The $3s \rightarrow 4d$ excitation is reduced, since only 31 of the 192 levels of the $3s3p^53d4d$ configuration are autoionizing. The ratio of metastable states in the $3s^23p^53d$ excited configuration to all states in the excited and ground configurations is 0.84. The difference between the total and direct ionization cross sections in Fig. 13 from threshold to about 835 eV is due solely to the $3s \rightarrow n\ell$ excitations.

3.11 Ni¹¹⁺ Results

In Fig. 14 a configuration-average distorted-wave calculation for the $3s^23p^5$ ground configuration of Ni¹¹⁺ is presented. The calculation includes the $2p \rightarrow 3p$, $2p \rightarrow 3d$, $2p \rightarrow 4\ell$ ($\ell = 0,1,2,3$), $2s \rightarrow 3p$, and $2s \rightarrow 3d$ excitations and direct ionization of the 3p and 3s subshells.

In Fig. 15 a configuration-average distorted-wave calculation for the $3s^23p^43d$ excited configuration of Ni¹¹⁺ is presented. The calculation includes the $3s \rightarrow 4d$, $3s \rightarrow n\ell$ ($n = 5,6$ and $\ell = 0,1,2$), $2p \rightarrow 3p$, $2p \rightarrow 3d$, $2p \rightarrow 4\ell$ ($\ell = 0,1,2,3$), $2p \rightarrow 3p$, and $2s \rightarrow 3d$ excitations and direct ionization of the 3d, 3p, and 3s subshells. The largest excitation is $2p \rightarrow 3d$. The $3s \rightarrow 4d$ excitation is greatly reduced, since only 9 of the 452 levels of the $3s3p^43d4d$ configuration are autoionizing; in addition, 73 of the 107 levels of the $3s3p^43d5s$ configuration and 254 of the 303 levels of the

$3s3p^43d5p$ configuration are autoionizing. The ratio of metastable states in the $3s^23p^43d$ excited configuration to all states in the excited and ground configurations is 0.38. The 2s and 2p excitations appear in Fig. 15 only above 835 eV.

3.12 Ni^{12+} Results

In Fig. 16 the crossed-beams measurements of Wang, Rinn, and Gregory¹⁵ for Ni^{12+} are compared with a configuration-average distorted-wave calculation for the $3s^23p^4$ ground configuration. The calculation includes the $2p \rightarrow 3p$, $2p \rightarrow 3d$, $2p \rightarrow 4\ell$ ($\ell = 0,1,2,3$), $2s \rightarrow 3p$, and $2s \rightarrow 3d$ excitations and direct ionization of the 3p and 3s subshells. As can be seen, the experimental measurements are noticeably higher than the calculated cross section and the experimental ionization threshold appears to occur at about 50 to 60 eV below the calculated ground state threshold.

In Fig. 17 the crossed-beams measurements of Wang, Rinn, and Gregory¹⁵ for Ni^{12+} are compared with a configuration-average distorted-wave calculation for the $3s^23p^33d$ excited configuration. The calculation includes the $3s \rightarrow n\ell$ ($n = 5,6$ and $\ell = 0,1,2$), $2p \rightarrow 3p$, $2p \rightarrow 3d$, $2p \rightarrow 4\ell$ ($\ell = 0,1,2,3$), $2s \rightarrow 3p$, and $2s \rightarrow 3d$ excitations and direct ionization of the 3d, 3p, and 3s subshells. The largest excitation is $2p \rightarrow 3d$. The ratio of metastable states in the $3s^23p^33d$ excited configuration to all states in the excited and ground configuration is 0.26. Experiment and theory agree quite well from threshold to an energy of approximately 750 eV. The lowest level of the $3s^23p^33d$ configuration lies about 55 eV above the ground state. The discrepancy from 750 eV to about 1080 eV may be at least partially due to the process of resonant recombination followed by double autoionization which is not included in these calculations. Nevertheless, the overall agreement between theory and experiment has improved, indicating that the initial population of the $3s^23p^33d$ excited configuration is quite high.

3.13 Ni^{13+} Results

In Fig. 18 a configuration-average distorted-wave calculation for the $3s^23p^3$ ground configuration of Ni^{13+} is presented. The calculation includes the $2p \rightarrow 3p$, $2p \rightarrow 3d$, $2p \rightarrow 4\ell$ ($\ell = 0,1,2,3$), $2s \rightarrow 3p$, and $2s \rightarrow 3d$ excitations and direct ionization of the 3p and 3s subshells.

In Fig. 19 a configuration-average distorted-wave calculation for the $3s^23p^23d$ ground configuration of Ni^{13+} is presented. The calculation includes the $3s \rightarrow n\ell$ ($n = 5,6$ and $\ell = 0,1,2$), $2p \rightarrow 3p$, $2p \rightarrow 3d$, $2p \rightarrow 4\ell$ ($\ell = 0,1,2,3$), $2s \rightarrow 3p$, and $2s \rightarrow 3d$ excitations and direct ionization of the 3d, 3p, and 3s subshells. The largest

excitation is $2p \rightarrow 3d$. The ratio of metastable states in the $3s^23p^23d$ excited configuration to all states in the excited and ground configurations is 0.12.

3.14 Ni¹⁴⁺ Results

In Fig. 20 the crossed-beams measurements of Wang, Rinn, and Gregory¹⁵ for Ni¹⁴⁺ are compared with a configuration-average distorted-wave calculation for the $3s^23p^2$ ground configuration. The calculation includes the $2p \rightarrow 3p$, $2p \rightarrow 3d$, $2p \rightarrow n\ell$ ($n = 4,5$ and $\ell = 0,1,2,3$), $2s \rightarrow 3p$, and $2p \rightarrow 3d$ excitations and direct ionization of the $3p$ and $3s$ subshells. Although the agreement between experiment and theory is not bad, the experimental onset of ionization appears to occur before the ionization threshold, and the measurements are consistently above the calculated cross section.

In Fig. 21 the crossed-beams measurements of Wang, Rinn, and Gregory¹⁵ for Ni¹⁴⁺ are compared with a configuration-average distorted-wave calculation for the $3s^23p3d$ excited configuration. The calculation includes the $3s \rightarrow 6\ell$ ($\ell = 0,1,2$), $2p \rightarrow 3p$, $2p \rightarrow 3d$, $2p \rightarrow n\ell$ ($n = 4,5$ and $\ell = 0,1,2,3$), $2s \rightarrow 3p$, and $2s \rightarrow 3d$ excitations and direct ionization of the $3d$, $3p$, and $3s$ subshells. The largest excitation is $2p \rightarrow 3d$. The ratio of the metastable state 3F_4 in the $3s^23p3d$ excited configuration to all states in the excited and ground configuration is 0.12. The agreement between experiment and theory is now much better. The theory is inside the error bars for the majority of the measurements. The two noticeably high points at 1034 and 1085 eV may be due to the process of resonant recombination followed by double autoionization. The comparison of the experimental measurements with theory in the case of Ni¹⁴⁺ may give the clearest evidence so far that the ECR ion source tends to populate metastable states, even for cases where theory predicts a very low metastable population on the basis of statistics alone.

3.15 Ni¹⁵⁺ Results

In Fig. 22 a configuration-average distorted-wave calculation for the $3s^23p$ ground configuration of Ni¹⁵⁺ is presented. The calculation includes the $2p \rightarrow 3p$, $2p \rightarrow 3d$, $2p \rightarrow n\ell$ ($n = 4,5$ and $\ell = 0,1,2,3$), $2s \rightarrow 3p$, and $2s \rightarrow 3d$ excitations and direct ionization of the $3p$ and $3s$ subshells. As can be seen, the excitation-autoionization contributions more than double the cross section by this stage of ionization.

3.16 Ni¹⁶⁺ Results

In Fig. 23 a distorted-wave calculation for the $3s^2$ ground configuration of Ni¹⁶⁺ is presented. The important $2p \rightarrow 3\ell$ ($\ell = 1,2$) excitations are calculated using a multiconfiguration level-to-level method; while the $2p \rightarrow n\ell$ ($n = 4,5$ and $\ell = 0,1,2,3$), $2s \rightarrow 3p$, $2s \rightarrow 3d$, and $2s \rightarrow 4\ell$ ($\ell = 0,1,2$) excitations and direct ionization of the $3s$ and $2p$ subshells are calculated using a configuration-average method. Correlation effects on excitation cross sections and branching ratios are significant for the $2p \rightarrow 3\ell$ excitations.

In Fig. 24 a distorted-wave calculation for the $3s3p$ excited configuration of Ni¹⁶⁺ is presented. The important $2p \rightarrow 3\ell$ ($\ell = 0,1,2$) excitations are calculated using a multiconfiguration level-to-level method; while the $2p \rightarrow n\ell$ ($n = 4,5$ and $\ell = 0,1,2,3$) and $2s \rightarrow n\ell$ ($n = 3,4$ and $\ell = 0,1,2$) excitations and direct ionization of the $3p$, $3s$, $2p$, and $2s$ subshells are calculated using a configuration-average method. As can be seen, in Figs. 23 and 24, the contributions from excitation-autoionization are now quite sizeable; near threshold the total cross section is about 4 times the direct cross section for $3s^2$, while this factor is about 3.5 in the case of $3s3p$.

3.17 Ni¹⁷⁺ Results

In Fig. 25 the multiconfiguration level-to-level distorted-wave results of Griffin, Pindzola, and Bottcher¹¹ for the $3s$ ground configuration of Ni¹⁷⁺ are presented. The calculation includes the $2p \rightarrow 3\ell$ ($\ell = 0,1,2$), $2p \rightarrow n\ell$ ($n = 4,5$ and $\ell = 1,2,3$), $2s \rightarrow 3\ell$ ($\ell = 0,1,2$), and $2s \rightarrow 4\ell$ ($\ell = 0,1,2,3$) excitations and direct ionization of the $3s$, $2p$, and $2s$ subshells. As can be seen, the ratio of the total ionization cross section to the direct ionization contribution is about 7 to 1 near threshold.

3.18 Ni¹⁸⁺ through Ni²⁶⁺ Results

For Ni¹⁸⁺ through Ni²⁶⁺ the contributions of excitation-autoionization to the total ionization cross section from the ground configuration should be less than 5%. For electron ionization from the ground configuration, the direct configuration-average cross section results of Table 1 should give a reasonable estimate of the total cross section and rate coefficient. Work is in progress on cross sections and rates from excited configurations of these same ions.

4. RATE COEFFICIENTS FOR Ni ATOMIC IONS

Rate coefficients for Ni^+ through Ni^{17+} were calculated using the theoretical and experimental cross section data discussed in the previous section. The theoretical results are presented in Tables 2-4 and Figs. 26-28, while the experimental results are presented in Table 5 and Fig. 29. The experimental cross section measurements were extrapolated to high energies in order to provide data over a sufficient energy range for these rate coefficient calculations.

In addition to the tabulated values and figure curves, a set of fitting parameters A_0 through A_8 are included in Tables 2-5. The natural logarithms of the rate coefficients are fitted to a Chebyshev polynomial expansion following the method of Cox and Hayes.¹⁶ One can then obtain the rate coefficients for any temperature kT from E_{\min} to E_{\max} using the equation

$$\alpha(kT) = \exp \left[\frac{A_0}{2} + \sum_{n=1}^8 A_n T_n(x) \right] , \quad (7)$$

where α is in units of cm^3/sec , $T_n(x)$ are the Chebyshev polynomials of the first kind,¹⁷ and x is defined by the equation

$$x = \ln \left[\frac{(kT)^2}{E_{\min} E_{\max}} \right] / \ln \left[\frac{E_{\max}}{E_{\min}} \right] , \quad (8)$$

with kT , E_{\min} , and E_{\max} in units of eV.

Our recommendation for Ni isonuclear rate coefficients is to use the experimental results for Ni^+ , Ni^{3+} , Ni^{5+} , Ni^{6+} , Ni^{7+} , Ni^{8+} , Ni^{12+} , and Ni^{14+} ; the ground configuration theoretical results for Ni^{2+} , Ni^{4+} , Ni^{9+} , Ni^{15+} , and Ni^{17+} ; excited configuration theoretical results for Ni^{10+} , Ni^{11+} , Ni^{13+} , and Ni^{16+} ; and the ground configuration direct only theoretical results from Table 1 for Ni^{18+} through Ni^{26+} . These recommended rates are incorporated in a subroutine called NIRATE (Q,TEMP), which will return the rate coefficient in cm^3/sec for any ionic charge Q and Temperature, TEMP, in electron volts. It will be available as a library function in directory /256/ATOMIC at the National Magnetic Fusion Energy Computer Center in Livermore, California. A listing of a program, written in BASIC, that produces rates using the given Chebyshev coefficients is found in Table 6.

ACKNOWLEDGMENTS

We wish to thank R. D. Cowan for making his atomic structure programs available to us and C. Bottcher for his development of the level-to-level distorted wave code used for part of this analysis. We also wish to thank all the members of the ORNL experimental team, in particular R. A. Phaneuf, for many valuable discussions.

REFERENCES

1. D. C. Gregory, F. W. Meyer, A. Müller, and P. Defrance, Phys. Rev. A 34, 3657 (1986).
2. M. S. Pindzola, D. C. Griffin, and C. Bottcher, Phys. Rev. A 34, 3668 (1986).
3. D. C. Gregory, L. J. Wang, F. W. Meyer, and K. Rinn, Phys. Rev. A 35, 3256 (1987).
4. M. S. Pindzola, D. C. Griffin, C. Bottcher, S. M. Younger, and H. T. Hunter, *Electron-Impact Ionization Data for the Fe Isonuclear Sequence*, ORNL/TM-10297, Martin Marietta Energy Systems, Inc., Oak Ridge Natl. Lab., Nov. 1987.
5. G. H. Dunn, p. 277 in *Electron Impact Ionization*, ed. T. D. Mark and G. H. Dunn (Springer-Verlag), New York, 1985.
6. S. M. Younger, Phys. Rev. A 22, 111 (1980).
7. H. Jakubowicz and D. L. Moores, J. Phys. B 14, 3733 (1981).
8. M. S. Pindzola, D. C. Griffin, and C. Bottcher, J. Phys. B 16, L355 (1983).
9. R. D. Cowan, *The Theory of Atomic Structure and Spectra* (University of California Press, Berkeley, 1981).
10. M. S. Pindzola, D. C. Griffin, and C. Bottcher, Phys. Rev. A 33, 3787 (1986).
11. D. C. Griffin, M. S. Pindzola, and C. Bottcher, Phys. Rev. A 36, 3642 (1987).
12. R. G. Montague and M.F.A. Harrison, J. Phys. B 18, 1419 (1985).
13. P. G. Burke, W. C. Fon, and A. E. Kingston, J. Phys. B 20, 2579 (1987).
14. D. C. Gregory and A. M. Howald, Phys. Rev. A 34, 97 (1986).
15. L. J. Wang, K. Rinn, and D. C. Gregory, J. Phys. B 21, 2117 (1988).
16. M. G. Cox and J. G. Hayes, U. K. National Physical Laboratory Report No. NAC 26, 1973.
17. M. Abramowitz and I. A. Stegun, p. 795 in *Handbook of Mathematical Functions* (Dover), New York, 1970.

Table 1. Direct ionization cross section parameters for ground and excited configurations in units of 10^{-14} ($\text{eV}^2 \cdot \text{cm}^2$)

Ion	Configuration	Subshell	I(eV)	A	B	C	D
Ni ⁺	$3s^2 3p^6 3d^9$	3d	18.15	-3.65	-23.20	25.08	-4.48
Ni ²⁺	$3s^2 3p^6 3d^8$	3d	36.16	5.25	-22.73	32.27	-23.78
Ni ³⁺	$3s^2 3p^6 3d^7$	3d	54.90	55.67	-43.21	31.58	-71.45
		3p	126.52	114.04	-56.05	8.90	-108.80
Ni ⁴⁺	$3s^2 3p^6 3d^6$	3d	79.08	67.81	-39.17	28.85	-75.70
		3p	149.27	86.76	-33.94	10.07	-81.76
Ni ⁵⁺	$3s^2 3p^6 3d^5$	3d	104.21	52.69	-23.15	22.80	-52.98
		3p	173.87	68.58	-20.77	10.88	-61.32
		3s	221.53	14.35	-1.79	2.65	-11.73
Ni ⁶⁺	$3s^2 3p^6 3d^4$	3d	131.35	38.07	-12.40	16.38	-32.16
		3p	200.15	63.13	-17.65	11.35	-52.65
		3s	248.55	13.77	-1.46	2.65	-10.07
Ni ⁷⁺	$3s^2 3p^6 3d^3$	3d	160.39	29.92	-8.59	10.68	-21.18
		3p	228.02	62.39	-18.22	11.54	-48.89
		3s	277.13	14.99	-2.49	2.64	-10.36
Ni ⁸⁺	$3s^2 3p^6 3d^2$	3d	191.25	22.05	-6.37	6.09	-13.89
		3p	257.38	62.34	-19.01	11.51	-46.43
		3s	307.18	16.99	-4.05	2.62	-11.62
Ni ⁹⁺	$3s^2 3p^6 3d$	3d	223.90	11.83	-3.43	2.58	-6.87
		3p	288.19	62.22	-19.42	11.33	-44.43
		3s	338.64	17.69	-4.81	2.60	-11.79
Ni ¹⁰⁺	$3s^2 3p^6$	3p	320.39	59.96	-18.39	10.01	-4.07
		3s	371.45	17.82	-5.18	2.57	-11.53

Table 1 (Continued)

Ion	Configuration	Subshell	I(eV)	A	B	C	D
Ni ¹⁰⁺	3s ² 3p ⁵ 3d	3d	256.10	12.80	-3.82	2.10	-7.21
		3p	320.34	50.17	-15.40	9.15	-34.07
		3s	368.42	15.94	-4.14	2.55	-9.75
Ni ¹¹⁺	3s ² 3p ⁵	3p	353.67	54.81	-18.06	8.85	-3.76
		3s	402.25	16.73	-4.74	2.51	-10.25
Ni ¹¹⁺	3s ² 3p ⁴ 3d	3d	289.43	12.85	-3.74	1.77	-6.82
		3p	353.46	43.97	-14.50	7.06	-30.13
		3s	399.02	15.73	-4.18	2.48	-9.30
Ni ¹²⁺	3s ² 3p ⁴	3p	387.90	44.35	-14.59	6.80	-2.97
		3s	433.85	14.28	-3.51	2.45	-7.64
Ni ¹²⁺	3s ² 3p ³ 3d	3d	323.87	12.78	-3.60	1.51	-6.43
		3p	387.52	33.40	-11.02	5.09	-22.39
		3s	430.42	14.17	-3.44	2.41	-7.57
Ni ¹³⁺	3s ² 3p ³	3p	423.04	32.29	-10.25	4.89	-2.07
		3s	466.24	16.17	-4.84	2.38	-9.35
Ni ¹³⁺	3s ² 3p ² 3d	3d	359.39	12.87	-3.60	1.29	-6.30
		3p	422.50	21.73	-6.95	3.25	-1.40
		3s	462.62	16.15	-4.86	2.35	-9.37
Ni ¹⁴⁺	3s ² 3p ²	3p	459.11	21.43	-6.70	3.12	-13.38
		3s	499.42	18.67	-6.48	2.31	-11.71
Ni ¹⁴⁺	3s ² 3p3d	3d	396.00	12.91	-3.59	1.12	-6.17
		3p	458.41	10.79	-3.39	1.56	-6.76
		3s	495.61	18.94	-6.66	2.28	-12.02
Ni ¹⁵⁺	3s ² 3p	3p	496.08	11.53	-3.75	1.49	-7.36
		3s	533.36	20.27	-7.75	2.25	-13.16
Ni ¹⁶⁺	3s ²	3s	568.08	17.81	-6.28	2.19	-10.73

Table 1 (Continued)

Ion	Configuration	Subshell	I(eV)	A	B	C	D
Ni ¹⁶⁺	3s3p	3p	530.80	9.56	-2.63	1.40	-5.24
		3s	572.17	8.97	-3.16	1.11	-5.40
Ni ¹⁷⁺	2s ² 2p ⁶ 3s	3s	607.48	9.06	-3.23	1.08	-5.47
		2p	1495.1	74.33	-24.32	10.70	-48.50
		2s	1642.9	16.35	-5.09	3.62	-11.70
Ni ¹⁸⁺	2s ² 2p ⁶	2p	1546.4	71.69	-23.19	10.71	-45.63
		2s	1692.1	16.33	-5.04	3.52	-11.47
Ni ¹⁹⁺	2s ² 2p ⁵	2p	1655.5	61.24	-19.16	7.78	-38.09
		2s	1786.4	16.49	-5.11	3.44	-11.41
Ni ²⁰⁺	2s ² 2p ⁴	2p	1667.6	49.29	-15.28	5.77	-30.11
		2s	1882.9	16.36	-4.97	3.35	-11.09
Ni ²¹⁺	2s ² 2p ³	2p	1882.5	37.12	-11.41	4.02	-22.30
		2s	2179.8	16.08	-4.74	3.26	-10.62
Ni ²²⁺	2s ² 2p ²	2p	2000.3	24.76	-7.54	2.50	-14.64
		2s	2082.6	15.74	-4.47	3.18	-10.13
Ni ²³⁺	2s ² 2p	2p	2121.0	13.41	-3.76	1.16	-7.24
		2s	2185.6	15.52	-4.27	3.09	-9.74
Ni ²⁴⁺	2s ²	2s	2290.9	15.46	-4.18	3.01	-9.52
Ni ²⁵⁺	1s ² 2s	2s	2401.2	7.82	-2.13	1.48	-4.77
		1s	10150	23.37	-9.12	4.02	-19.82
Ni ²⁶⁺	1s ²	1s	10299	23.27	-8.97	3.92	-19.55

Table 2. Theoretical electron-impact ionization rate coefficients for Ni⁺ through Ni⁹⁺ in ground configurations. A₀ through A₈ are Chebyshev fitting parameters which can be used to calculate rate coefficients at any value of kT between E_{min} and E_{max} (in eV).

kT (eV)	Ni ⁺	Ni ²⁺	Ni ³⁺	Ni ⁴⁺	Ni ⁵⁺
4	0.377E-09				
7	0.339E-08	0.912E-10			
10	0.837E-08	0.508E-09	0.588E-10		
20	0.252E-07	0.436E-08	0.133E-08	0.433E-09	0.706E-10
40	0.460E-07	0.144E-07	0.698E-08	0.313E-08	0.116E-08
70	0.608E-07	0.253E-07	0.151E-07	0.791E-08	0.403E-08
100	0.683E-07	0.320E-07	0.209E-07	0.118E-07	0.674E-08
200	0.772E-07	0.423E-07	0.310E-07	0.194E-07	0.125E-07
400	0.788E-07	0.470E-07	0.371E-07	0.249E-07	0.168E-07
700	0.760E-07	0.472E-07	0.386E-07	0.269E-07	0.185E-07
1000	0.727E-07	0.459E-07	0.382E-07	0.270E-07	0.187E-07
2000	0.646E-07	0.416E-07	0.352E-07	0.254E-07	0.177E-07
4000	0.555E-07	0.360E-07	0.307E-07	0.224E-07	0.156E-07
7000	0.480E-07	0.312E-07	0.266E-07	0.195E-07	0.136E-07
10000	0.434E-07	0.283E-07	0.241E-07	0.177E-07	0.122E-07
20000	0.351E-07	0.229E-07	0.194E-07	0.142E-07	0.982E-08
A ₀	-3.66635E+01	-3.76460E+01	-3.79681E+01	-3.85750E+01	-3.91743E+01
A ₁	2.25401E+00	2.27280E+00	2.22173E+00	2.15972E+00	2.01676E+00
A ₂	-2.43707E+00	-2.35146E+00	-2.29010E+00	-2.19591E+00	-2.13163E+00
A ₃	1.19271E+00	1.08800E+00	1.05141E+00	9.68002E-01	9.64536E-01
A ₄	-5.65630E-01	-4.56723E-01	-4.42409E-01	-3.90634E-01	-3.96441E-01
A ₅	2.55951E-01	1.77111E-01	1.77389E-01	1.54522E-01	1.54723E-01
A ₆	-1.05624E-01	-6.33619E-02	-6.77278E-02	-6.05860E-02	-5.56487E-02
A ₇	3.58266E-02	1.96560E-02	2.24215E-02	2.10912E-02	1.64365E-02
A ₈	-9.19214E-03	-4.98623E-03	-6.04353E-03	-6.22187E-03	-3.25822E-03
E _{min}	2.34823E+00	5.02809E+00	7.79442E+00	1.00463E+01	1.47345E+01
E _{max}	1.00000E+05	1.00000E+05	1.00000E+05	1.00000E+05	1.00000E+05

Table 2 (Continued)

kT (eV)	Ni ⁶⁺	Ni ⁷⁺	Ni ⁸⁺	Ni ⁹⁺
20	0.130E-10	0.241E-11		
40	0.411E-09	0.155E-09	0.461E-10	0.145E-10
70	0.189E-08	0.945E-09	0.401E-09	0.179E-09
100	0.352E-08	0.197E-08	0.961E-09	0.491E-09
200	0.740E-08	0.470E-08	0.270E-08	0.162E-08
400	0.107E-07	0.722E-08	0.451E-08	0.298E-08
700	0.121E-07	0.845E-08	0.548E-08	0.380E-08
1000	0.125E-07	0.880E-08	0.580E-08	0.413E-08
2000	0.121E-07	0.866E-08	0.581E-08	0.435E-08
4000	0.108E-07	0.781E-08	0.529E-08	0.418E-08
7000	0.945E-08	0.687E-08	0.468E-08	0.389E-08
10000	0.858E-08	0.624E-08	0.426E-08	0.368E-08
20000	0.695E-08	0.505E-08	0.346E-08	0.322E-08
A ₀	-3.97758D+01	-4.11488D+01	-4.18260D+01	-4.21495D+01
A ₁	1.90654D+00	2.54999D+00	2.45873D+00	2.59824D+00
A ₂	-2.00215D+00	-2.45092D+00	-2.35509D+00	-2.19817D+00
A ₃	8.99513D-01	1.14157D+00	1.08660D+00	1.04048D+00
A ₄	-3.63967D-01	-4.80538D-01	-4.48140D-01	-4.30821D-01
A ₅	1.38502D-01	1.87510D-01	1.70502D-01	1.56374D-01
A ₆	-4.88968D-02	-6.60528D-02	-5.91575D-02	-5.40717D-02
A ₇	1.44073D-02	1.91574D-02	1.71917D-02	1.72057D-02
A ₈	-2.91663D-03	-3.92451D-03	-3.40225D-03	-3.62183D-03
E _{min}	1.94347D+01	1.83878D+01	2.29468D+01	2.75983D+01
E _{max}	1.00000D+05	1.00000D+05	1.00000D+05	1.00000D+05

Table 3. Theoretical electron-impact ionization rate coefficients for Ni¹⁰⁺ through Ni¹⁷⁺ in ground configurations. A₀ through A₈ are Chebyshev fitting parameters which can be used to calculate rate coefficients at any value of kT between E_{min} and E_{max} (in eV).

kT (eV)	Ni ¹⁰⁺ (3p ⁶)	Ni ¹¹⁺ (3p ⁵)	Ni ¹²⁺ (3p ⁴)	Ni ¹³⁺ (3p ³)
70	0.147E-10	0.671E-11	0.299E-11	0.119E-11
100	0.667E-10	0.353E-10	0.183E-10	0.866E-11
200	0.417E-09	0.265E-09	0.167E-09	0.102E-09
400	0.109E-08	0.777E-09	0.542E-09	0.387E-09
700	0.165E-08	0.124E-08	0.908E-09	0.695E-09
1000	0.192E-08	0.148E-08	0.110E-08	0.867E-09
2000	0.219E-08	0.174E-08	0.132E-08	0.107E-08
4000	0.216E-08	0.174E-08	0.133E-08	0.110E-08
7000	0.199E-08	0.162E-08	0.125E-08	0.104E-08
10000	0.185E-08	0.151E-08	0.117E-08	0.975E-09
20000	0.154E-08	0.127E-08	0.978E-09	0.825E-09
A ₀	-4.34929D+01	-4.38220E+01	-4.42682E+01	-4.45804E+01
A ₁	2.37145D+00	2.29690E+00	2.22281E+00	2.18514E+00
A ₂	-2.11061D+00	-2.02628E+00	-1.96603E+00	-1.90788E+00
A ₃	8.92249D-01	8.37964E-01	8.03011E-01	7.69567E-01
A ₄	-3.32325D-01	-3.02312E-01	-2.82754E-01	-2.60756E-01
A ₅	1.12536D-01	9.81709E-02	8.66540E-02	7.17096E-02
A ₆	-3.59692D-02	-3.10159E-02	-2.52266E-02	-1.70567E-02
A ₇	1.10547D-02	1.02622E-02	8.19505E-03	4.98693E-03
A ₈	-3.38784D-03	-3.97595E-03	-3.95725E-03	-3.56403E-03
E _{min}	4.54271D+01	5.26554E+01	5.99177E+01	6.94518E+01
E _{max}	1.00000D+05	1.00000E+05	1.00000E+05	1.00000E+05

Table 3 (Continued)

kT (eV)	Ni ¹⁴⁺ (3p ²)	Ni ¹⁵⁺ (3p)	Ni ¹⁶⁺ (3s ²)	Ni ¹⁷⁺ (2s ² 2p ⁶ 3s)
70	0.473E-12	0.167E-12		
100	0.413E-11	0.180E-11	0.614E-12	0.223E-12
200	0.625E-10	0.378E-10	0.206E-10	0.104E-10
400	0.276E-09	0.197E-09	0.138E-09	0.818E-10
700	0.531E-09	0.400E-09	0.312E-09	0.204E-09
1000	0.680E-09	0.522E-09	0.424E-09	0.294E-09
2000	0.860E-09	0.677E-09	0.581E-09	0.445E-09
4000	0.896E-09	0.718E-09	0.638E-09	0.532E-09
7000	0.854E-09	0.692E-09	0.624E-09	0.552E-09
10000	0.806E-09	0.657E-09	0.596E-09	0.545E-09
20000	0.684E-09	0.563E-09	0.516E-09	0.499E-09
A ₀	-4.58933E+01	-4.62552E+01	-4.63945E+01	-4.65892E+01
A ₁	3.00409E+00	2.97346E+00	2.92112E+00	2.28453E+00
A ₂	-2.42796E+00	-2.38466E+00	-2.32119E+00	-2.39389E+00
A ₃	1.00956E+00	9.95441E-01	9.63562E-01	1.14118E+00
A ₄	-3.46325E-01	-3.39889E-01	-3.29972E-01	-4.86274E-01
A ₅	9.35175E-02	8.28793E-02	7.94690E-02	1.84636E-01
A ₆	-2.27503E-02	-9.86203E-03	-4.06391E-03	-5.65652E-02
A ₇	8.17149E-03	-6.46052E-04	-6.27780E-03	1.06504E-02
A ₈	-6.58973E-03	-2.14704E-03	2.54280E-03	2.92630E-03
E _{min}	5.77462E+01	6.57106E+01	7.90307E+01	9.10000E+01
E _{max}	1.00000E+05	1.00000E+05	1.00000E+05	1.00000E+06

Table 4. Theoretical electron-impact ionization rate coefficients for Ni¹⁰⁺ through Ni¹⁴⁺ and Ni¹⁶⁺ in excited configuration. A₀ through A₈ are Chebyshev fitting parameters which can be used to calculate rate coefficients at any value of kT between E_{min} and E_{max} (in eV).

kT (eV)	Ni ¹⁰⁺ (3p ⁵ 3d)	Ni ¹¹⁺ (3p ⁴ 3d)	Ni ¹²⁺ (3p ³ 3d)	Ni ¹³⁺ (3p ² 3d)
40	0.135E-11			
70	0.303E-10	0.172E-11	0.741E-11	0.307E-11
100	0.113E-09	0.699E-10	0.343E-11	0.170E-10
200	0.568E-09	0.394E-09	0.231E-10	0.145E-09
400	0.134E-08	0.100E-09	0.656E-09	0.473E-09
700	0.194E-08	0.150E-08	0.104E-08	0.798E-09
1000	0.222E-08	0.174E-08	0.124E-08	0.972E-09
2000	0.246E-08	0.198E-08	0.145E-08	0.116E-08
4000	0.238E-08	0.194E-08	0.144E-08	0.117E-08
7000	0.218E-08	0.178E-08	0.134E-08	0.109E-08
10000	0.201E-08	0.165E-08	0.125E-08	0.102E-08
20000	0.167E-08	0.137E-08	0.104E-08	0.857E-09
A ₀	-4.33524E+01	-4.36978E+01	-4.42060E+01	-4.45228E+01
A ₁	2.40505E+00	2.35247E+00	2.28880E+00	2.21252E+00
A ₂	-2.15144E+00	-2.09190E+00	-2.01518E+00	-1.94726E+00
A ₃	9.02842E-01	8.65733E-01	8.12960E-01	7.77841E-01
A ₄	-3.27903E-01	-3.11149E-01	-2.79648E-01	-2.58932E-01
A ₅	1.06287E-01	1.01562E-01	8.53762E-02	7.15809E-02
A ₆	-3.16805E-02	-3.24382E-02	-2.69842E-02	-1.96727E-02
A ₇	8.90980E-03	1.06369E-02	1.01666E-02	7.56180E-03
A ₈	-2.19098E-03	-3.35400E-03	-4.57564E-03	-4.75867E-03
E _{min}	3.84743E+01	4.29800E+01	4.98190E+01	5.88219E+01
E _{max}	1.00000E+05	1.00000E+05	1.00000E+05	1.00000E+05

Table 4 (Continued)

kT (eV)	Ni ¹⁴⁺ (3p3d)	Ni ¹⁶⁺ (3s3p)
70	0.133E-11	
100	0.867E-11	0.885E-12
200	0.922E-10	0.244E-10
400	0.346E-09	0.153E-09
700	0.623E-09	0.344E-09
1000	0.777E-09	0.470E-09
2000	0.952E-09	0.655E-09
4000	0.970E-09	0.731E-09
7000	0.914E-09	0.723E-09
10000	0.857E-09	0.694E-09
20000	0.720E-09	0.605E-09
A ₀	-4.57567E+01	-4.62547E+01
A ₁	2.98174E+00	3.06484E+00
A ₂	-2.43670E+00	-2.36139E+00
A ₃	1.00131E+00	9.54352E-01
A ₄	-3.38721E-01	-3.15891E-01
A ₅	9.43743E-02	7.26676E-02
A ₆	-2.85781E-02	-3.27672E-03
A ₇	1.31372E-02	-5.30048E-03
A ₈	-8.53298E-03	9.61339E-04
E _{min}	4.98190E+01	7.34060E+01
E _{max}	1.00000E+05	1.00000E+05

Table 5. Experimental electron-impact ionization rate coefficients for various Ni ions. A_0 through A_8 are Chebyshev fitting parameters used to calculate the rate coefficient at any kT from E_{\min} to E_{\max} (in eV).

kT (eV)	Ni^+	Ni^{3+}	Ni^{5+}	Ni^{6+}	Ni^{7+}
10	0.666E-08	0.693E-10	0.365E-12	0.157E-13	0.816E-15
20	0.199E-07	0.112E-08	0.661E-10	0.119E-10	0.224E-11
30	0.302E-07	0.309E-08	0.399E-09	0.116E-09	0.358E-10
40	0.380E-07	0.533E-08	0.101E-08	0.369E-09	0.146E-09
70	0.532E-07	0.115E-07	0.350E-08	0.171E-08	0.907E-09
100	0.620E-07	0.162E-07	0.595E-08	0.325E-08	0.192E-08
150	0.705E-07	0.219E-07	0.924E-08	0.548E-08	0.351E-08
200	0.751E-07	0.257E-07	0.117E-07	0.720E-08	0.480E-08
300	0.793E-07	0.303E-07	0.148E-07	0.957E-08	0.663E-08
400	0.805E-07	0.329E-07	0.166E-07	0.111E-07	0.777E-08
700	0.786E-07	0.358E-07	0.185E-07	0.130E-07	0.921E-08
1000	0.751E-07	0.361E-07	0.185E-07	0.135E-07	0.945E-08
1500	0.699E-07	0.353E-07	0.177E-07	0.132E-07	0.912E-08
2000	0.658E-07	0.342E-07	0.169E-07	0.126E-07	0.860E-08
3000	0.598E-07	0.319E-07	0.154E-07	0.114E-07	0.771E-08
A_0	-3.45059E+01	-3.76222E+01	-4.11200E+01	-4.31480E+01	-4.51200E+01
A_1	1.29314E+00	2.61866E+00	4.39480E+00	5.53320E+00	6.57760E+00
A_2	-8.35410E-01	-1.37880E+00	-2.45420E+00	-3.06310E+00	-3.70010E+00
A_3	2.05560E-01	4.09000E-01	8.40810E-01	1.10400E+00	1.34790E+00
A_4	-6.43491E-02	-1.28846E-01	-2.82720E-01	-3.82580E-01	-4.47220E-01
A_5	2.79552E-02	3.95767E-02	8.78700E-02	1.03060E-01	1.08590E-01
A_6	-6.04574E-03	-7.30130E-03	-1.45300E-02	-1.77800E-02	-4.83000E-03
A_7	3.68188E-04	-3.22187E-04	1.44000E-03	4.86000E-03	-3.67000E-03
A_8	-1.07925E-03	1.06608E-05	-2.37000E-03	-1.70000E-03	9.80000E-04
E_{\min}	7.00000E+00	1.00000E+01	1.00000E+01	1.00000E+01	1.00000E+01
E_{\max}	3.00000E+03	3.00000E+03	3.00000E+03	3.00000E+03	3.00000E+03

Table 5 (Continued)

kT (eV)	Ni ⁸⁺	Ni ¹²⁺	Ni ¹⁴⁺
10	0.254E-15		
20	0.446E-12		
30	0.990E-11		
40	0.499E-10		
70	0.413E-09	0.621E-11	0.834E-12
100	0.980E-09	0.318E-10	0.669E-11
150	0.197E-08	0.120E-09	0.360E-10
200	0.283E-08	0.241E-09	0.870E-10
300	0.413E-08	0.500E-09	0.218E-09
400	0.500E-08	0.729E-09	0.348E-09
700	0.637E-08	0.118E-08	0.619E-09
1000	0.694E-08	0.141E-08	0.752E-09
1500	0.718E-08	0.156E-08	0.832E-09
2000	0.703E-08	0.160E-08	0.839E-09
3000	0.655E-08	0.155E-08	0.799E-09
A ₀	-4.66390E+01	-4.46378E+01	-4.68830E+01
A ₁	7.30100E+00	3.13794E+00	3.91127E+00
A ₂	-3.82440E+00	-1.36974E+00	-1.77077E+00
A ₃	1.28820E+00	3.25212E-01	4.27401E-01
A ₄	-3.09730E-01	-7.66653E-02	-9.63996E-02
A ₅	-1.92400E-02	1.75100E-02	2.75672E-02
A ₆	6.31500E-02	-3.79199E-03	-8.64076E-03
A ₇	-3.70500E-02	5.90838E-04	2.79192E-03
A ₈	1.44800E-02	7.40489E-04	4.98384E-04
E _{min}	1.00000E+01	5.50000E+01	5.50000E+01
E _{max}	3.00000E+03	3.00000E+03	3.00000E+03

Table 6. Sample BASIC program to calculate rate coefficients
from Chebyshev fitting parameters

```

10 REM PROGRAM CHEBFE
20 REM CHBFIT PROGRAM IS A BASIC PROGRAM DERIVED FROM A PROGRAM IN
30 REM "ELEMENTARY NUMERICAL ANALYSIS: AN ALGORITHMIC APPROACH", S.D. CONTE
40 REM AND C. DE BOOR, MCGRAW-HILL, INC., P 254, 1972.
50 DIM D(9)
60 NTERMS=9
70 INPUT"ENTER Emin (eV) ",EMIN:INPUT"ENTER Emax (eV) ",EMAX
80 EMINL=LOG(EMIN)
90 EMAXL=LOG(EMAX)
100 PRINT USING "ENTER # COEFFICIENTS A0 THROUGH A8; NTERMS"
110 FOR J=1 TO NTERMS
120 INPUT D(J):NEXT J
130 PRINT USING "INPUT ENERGY (eV) BETWEEN ##### AND ####. FOR THE RATE COEF.
CALCULATION";EMIN;EMAX
140 REM GET ENERGY FOR CALCULATION AND USE THREE TERM RECURRENCE RELATION
150 INPUT X
160 K=NTERMS
170 CHEB=D(K)
180 IF X<0 THEN END
190 X=LOG(X)
200 K=K-1
210 IF K=0 THEN END
220 XNORM=(X-EMINL-(EMAXL-X))/(EMAXL-EMINL)
230 TWOX=2*XNORM
240 PREV2=0
250 PREV=CHEB
260 IF K=1 GOTO 310
270 CHEB=D(K)+TWOX*PREV-PREV2
280 PREV2=PREV
290 K=K-1
300 GOTO 250
310 CHEB=.5*D(1)+XNORM*PREV-PREV2
320 PRINT USING "####.###... = RATE CHEB=EXP(CHEB) COEFFICIENT (CM3/S)";CHEB
330 GOTO 130
340 END

```

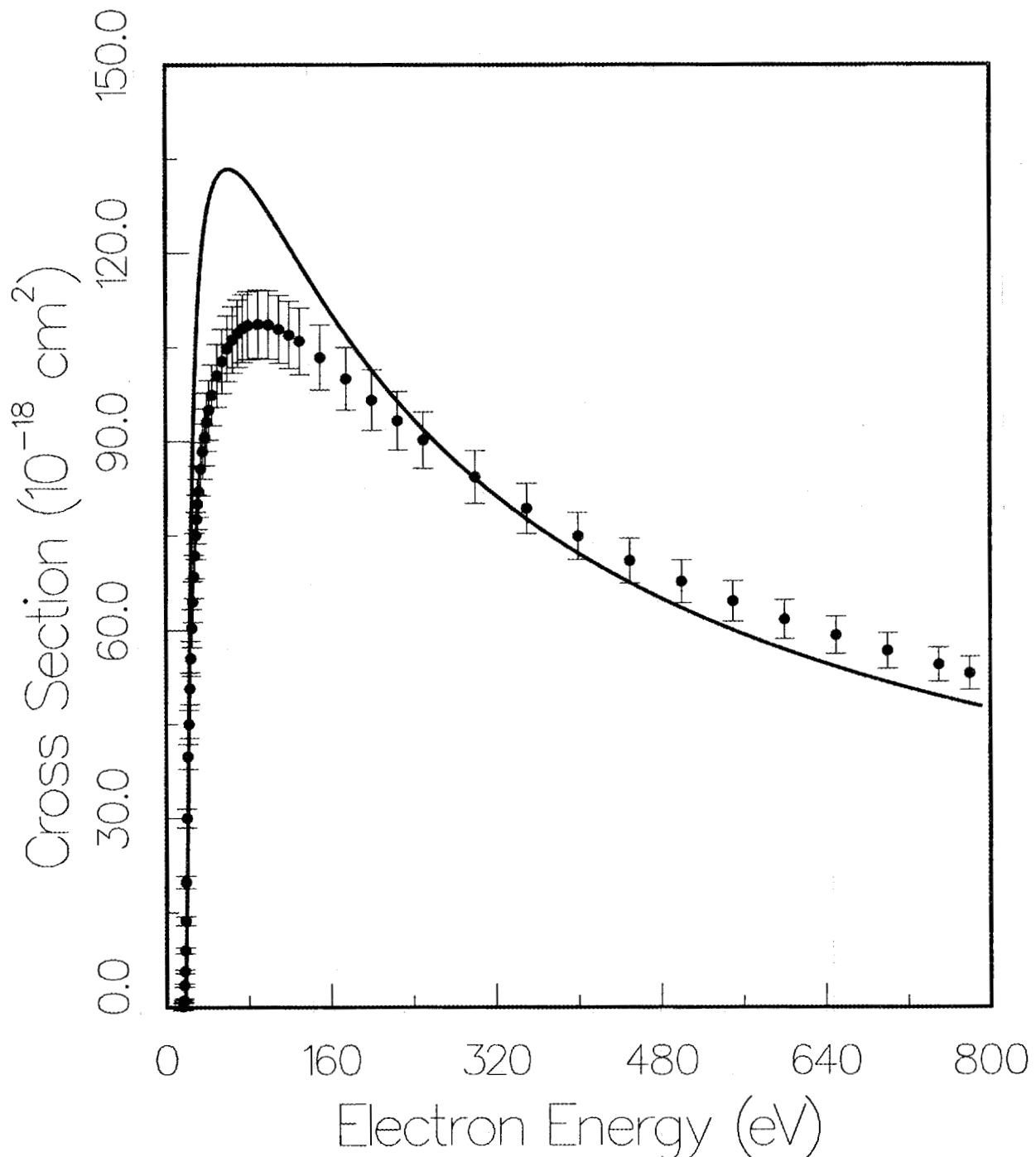
$\text{Ni}^+(3s23p63d9)$


Fig. 1. Electron-impact ionization of Ni^+ . Full curve, configuration-average direct ionization cross section from the $3d^9$ ground configuration; experimental points (ref. 12).

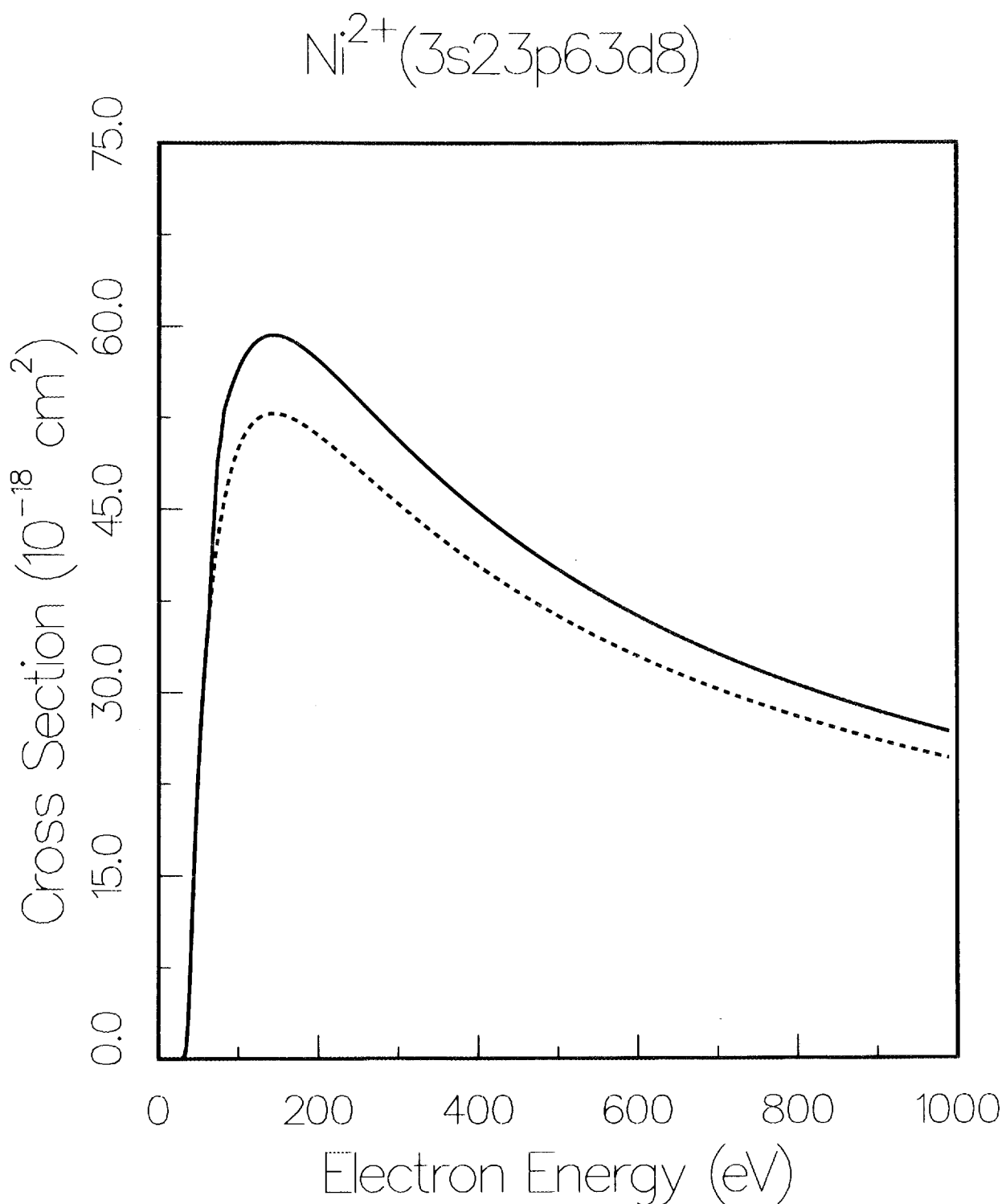


Fig. 2. Electron-impact ionization of Ni^{2+} . Full curve, configuration-average total ionization cross section from the $3d^8$ ground configuration; dashed curve, direct ionization cross section only.

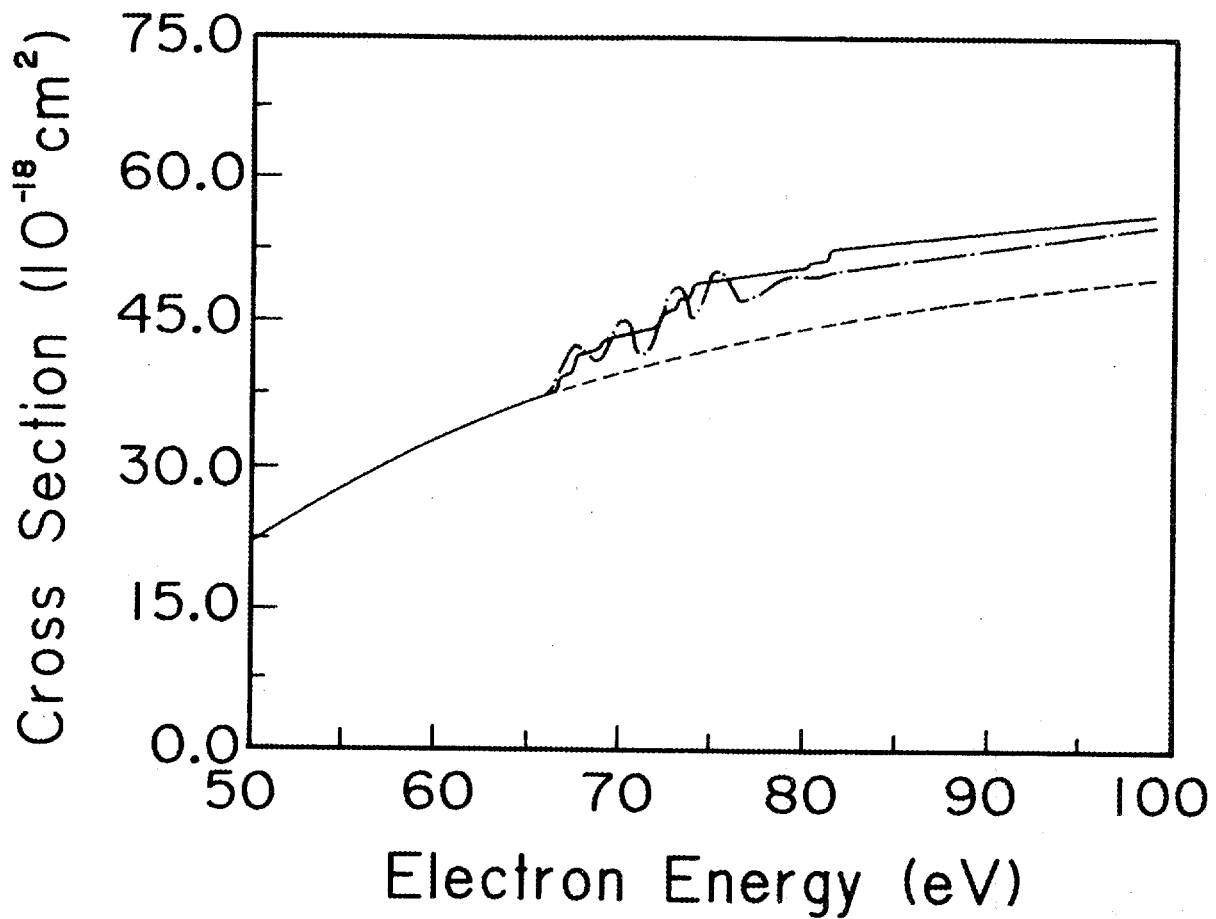


Fig. 3. Electron-impact ionization of Ni^{2+} below 100 eV. Full curve, configuration-average total ionization cross section from the $3d^8$ ground configuration; chained curve, R-matrix calculation (ref. 13); dashed curve, direct ionization cross section only.

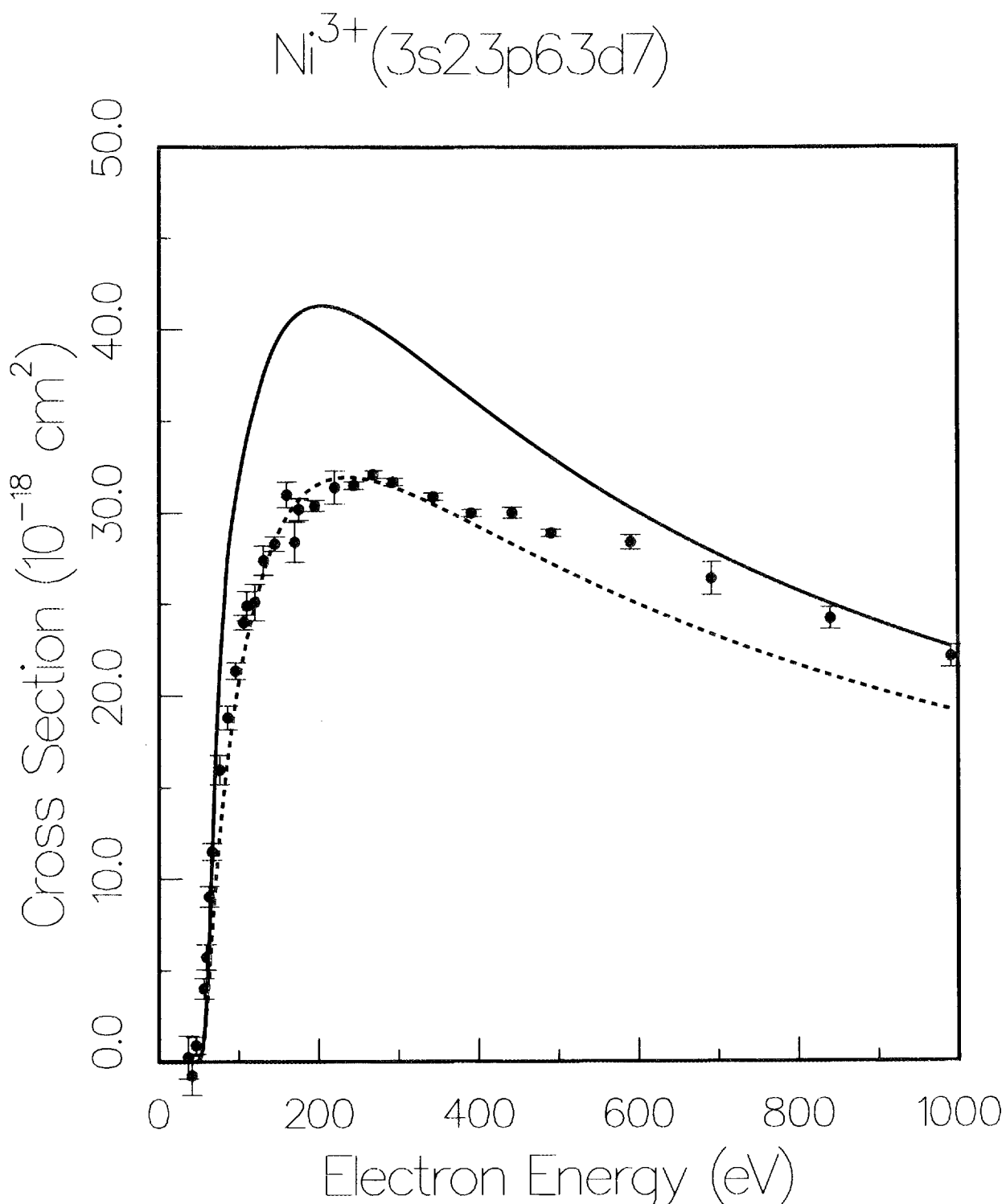


Fig. 4. Electron-impact ionization of Ni^{3+} . Full curve, configuration-average total ionization cross section from the $3d^7$ ground configuration; dashed curve, direct ionization cross section only; experimental points (ref. 14).

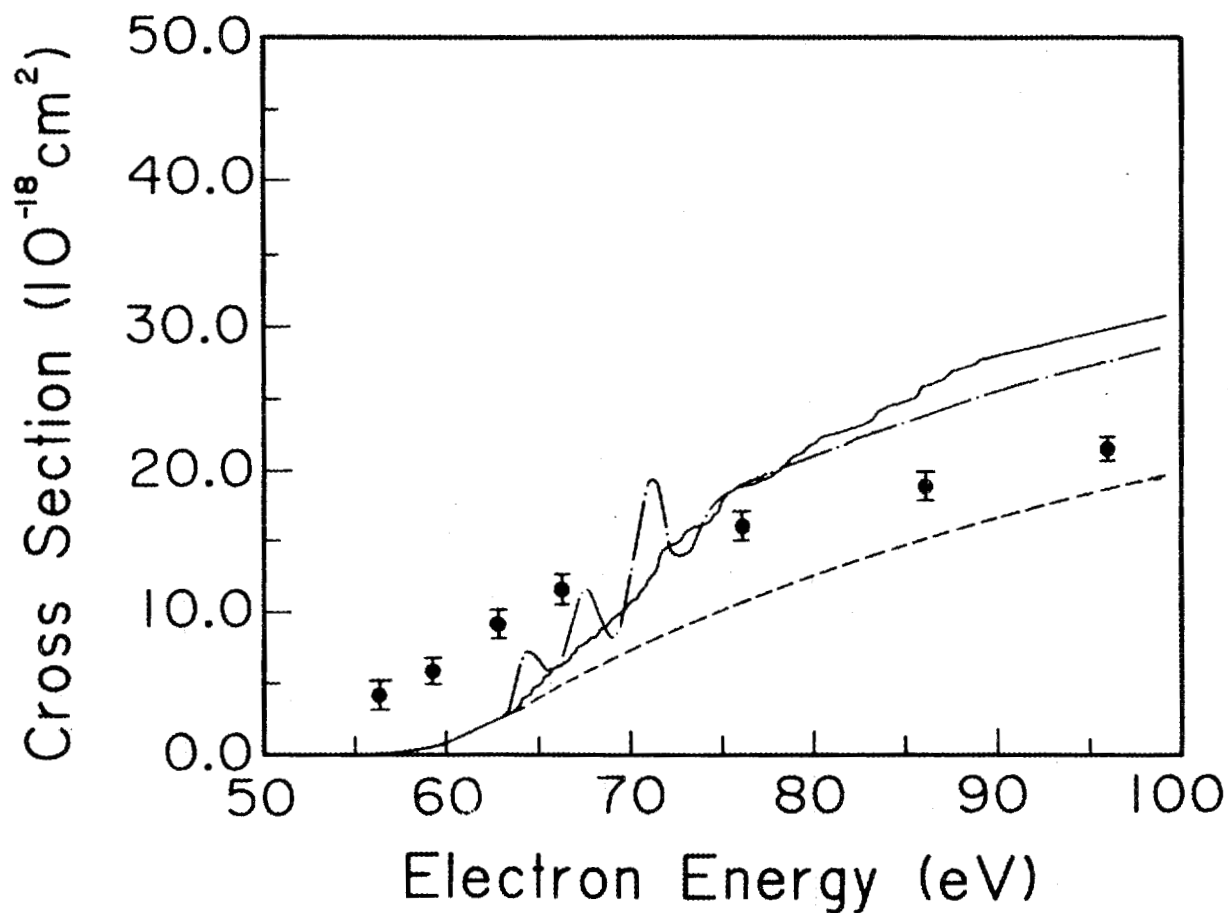


Fig. 5. Electron-impact ionization of Ni^{3+} below 100 eV. Full curve, configuration-average total ionization cross section from the $3d^7$ ground configuration; chained curve, R-matrix calculation (ref. 13); dashed curve, direct ionization cross section only; experimental points (ref. 14).

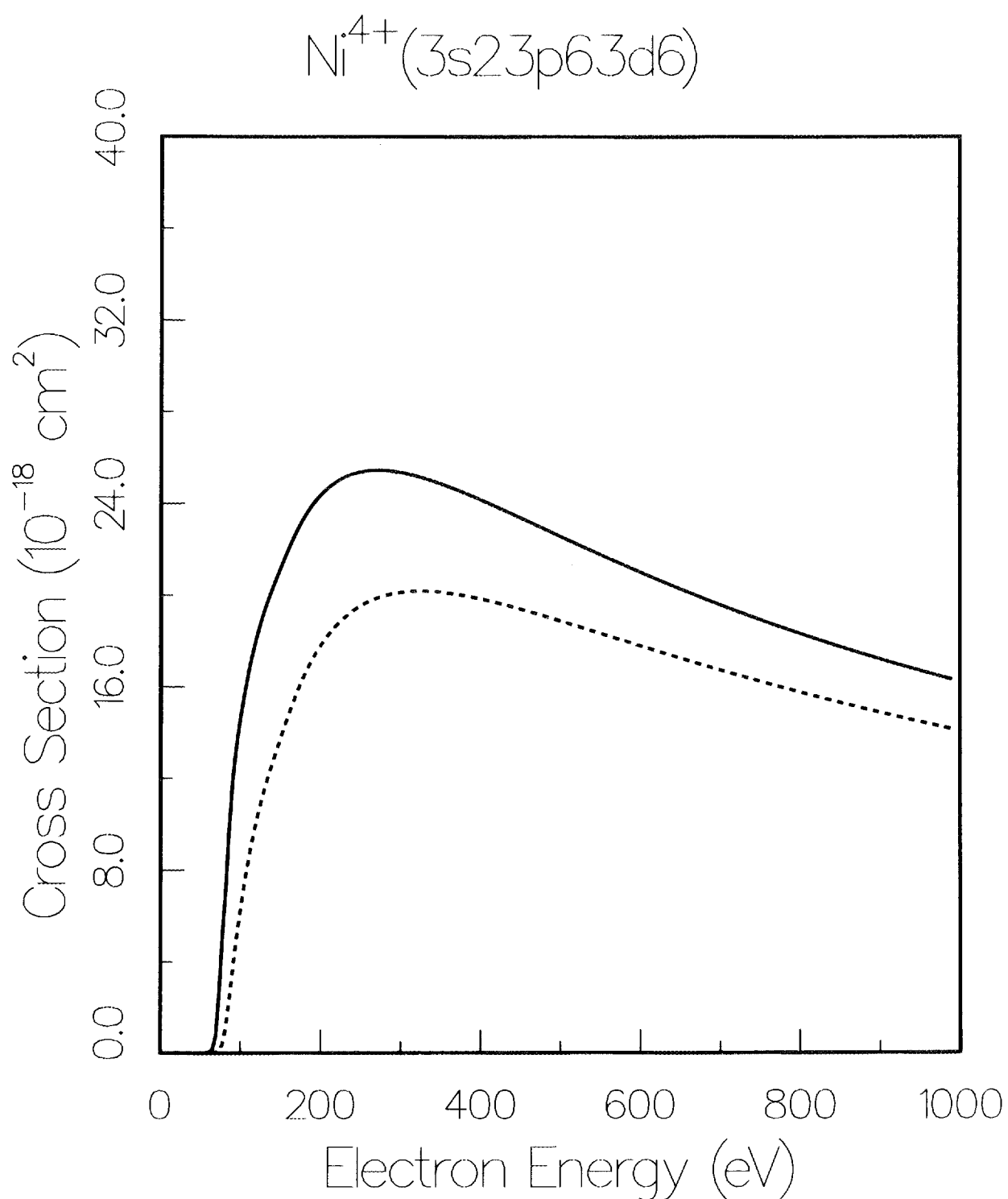


Fig. 6. Electron-impact ionization of Ni^{4+} . Full curve, configuration-average total ionization cross section from the $3d^6$ ground configuration; dashed curve, direct ionization cross section only.

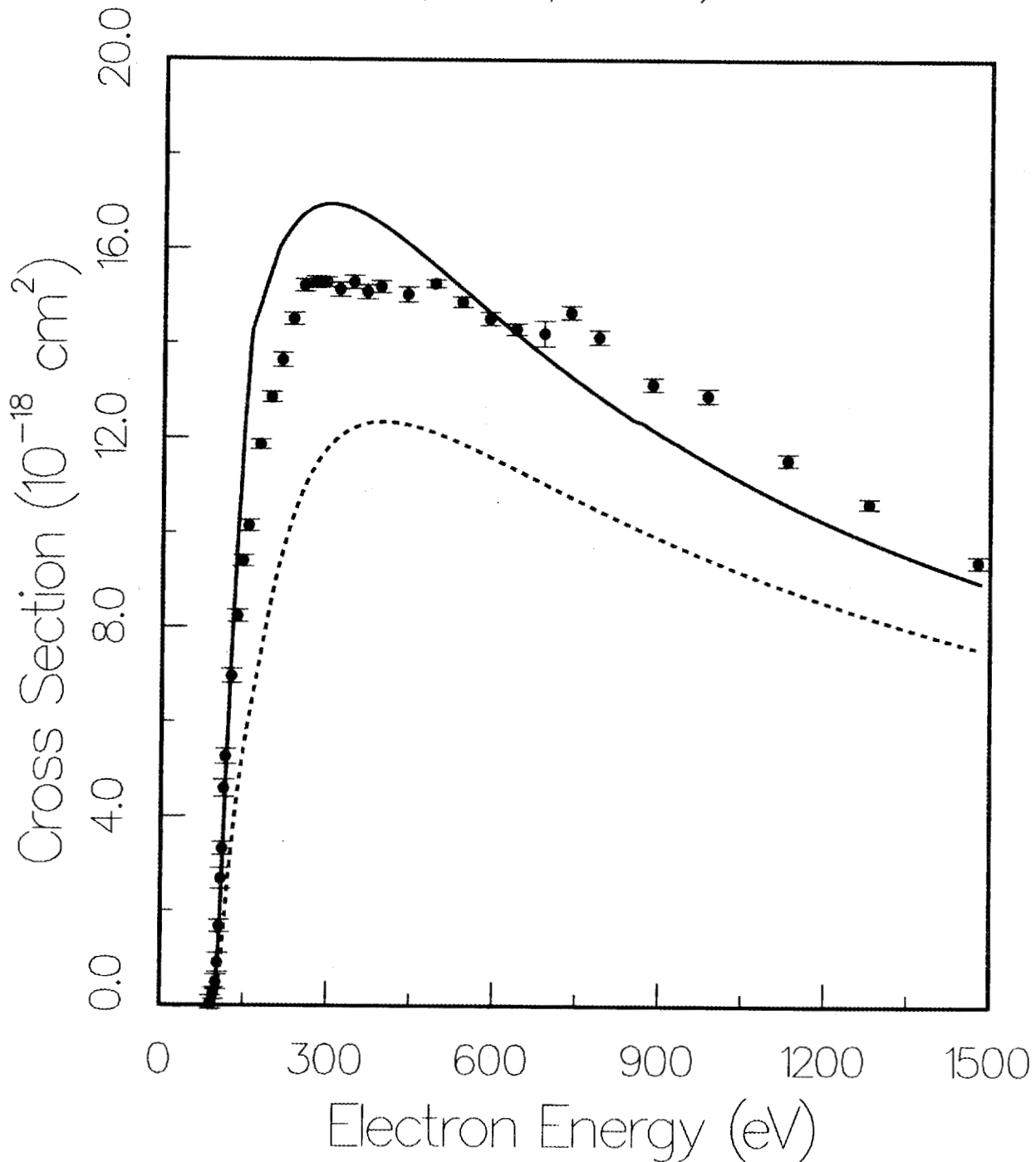
$Ni^{5+}(3s23p63d5)$


Fig. 7. Electron-impact ionization of Ni^{5+} . Full curve, configuration-average total ionization cross section from the $3d^5$ ground configuration; dashed curve, direct ionization cross section only; experimental points (ref. 15).

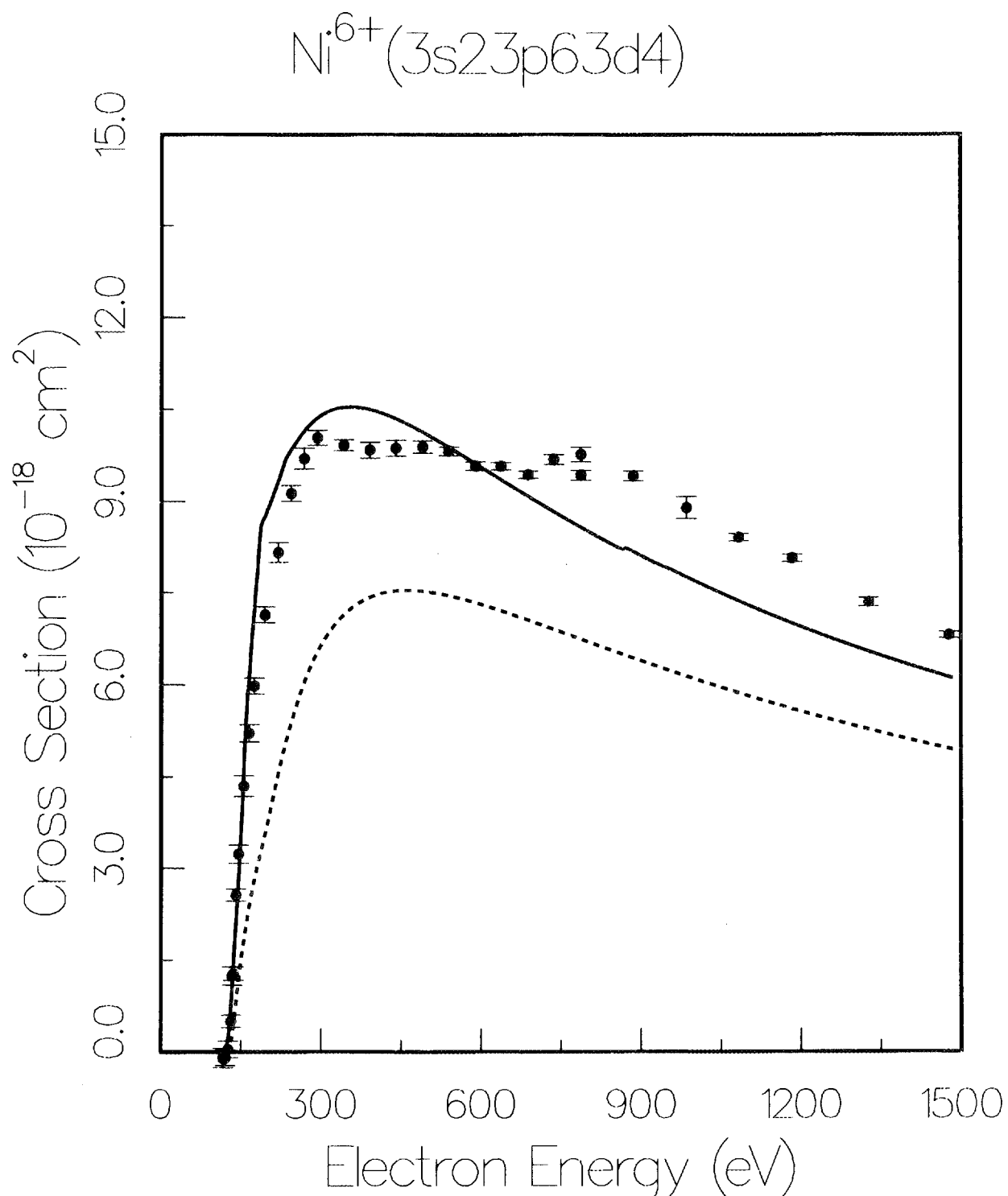


Fig. 8. Electron-impact ionization of Ni^{6+} . Full curve, configuration-average total ionization cross section from the $3d^4$ ground configuration; dashed curve, direct ionization cross section only; experimental points (ref. 15).

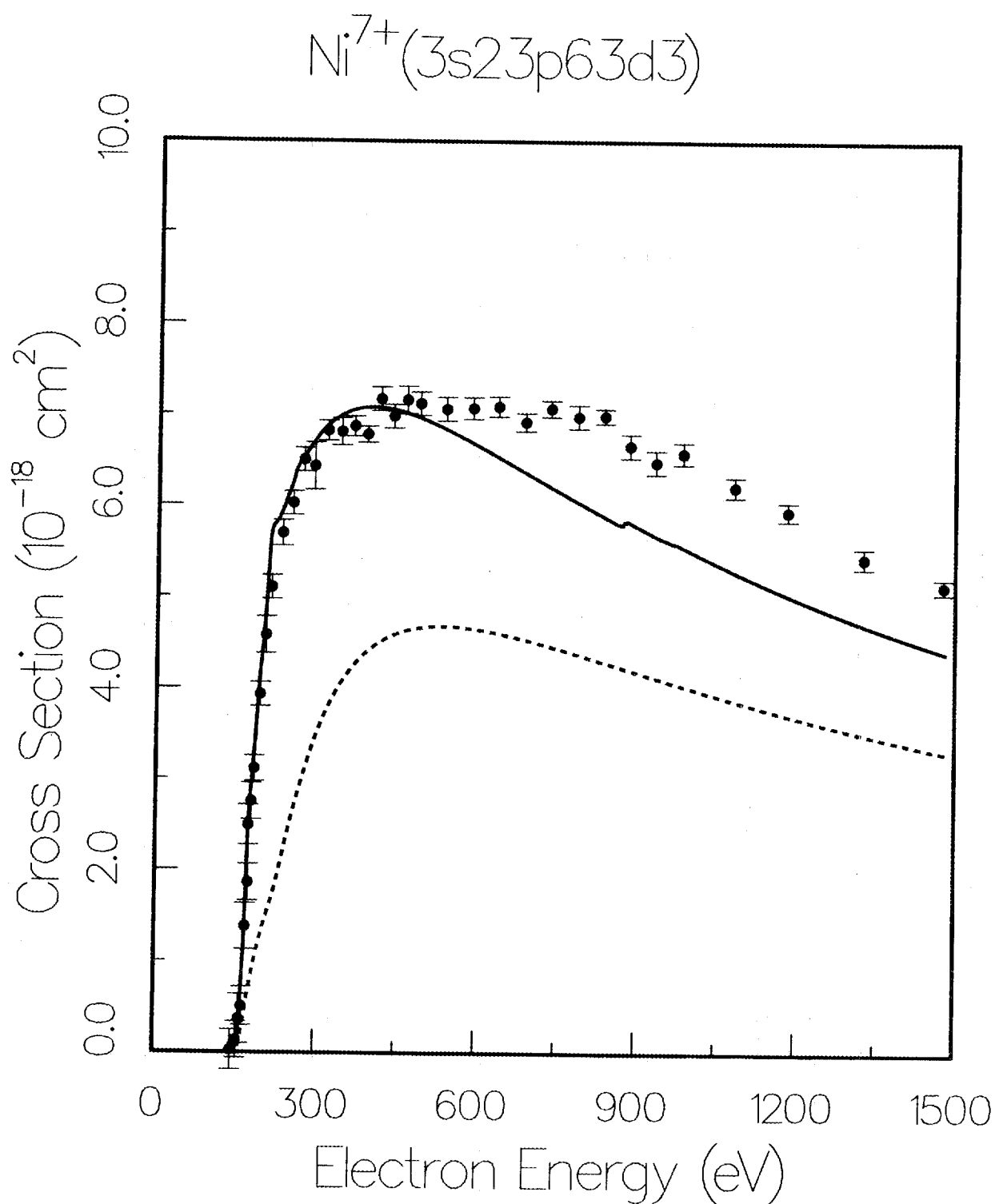


Fig. 9. Electron-impact ionization of Ni^{7+} . Full curve, configuration-average total ionization cross section from the $3d^3$ ground configuration; dashed curve, direct ionization cross section only; experimental points (ref. 15).

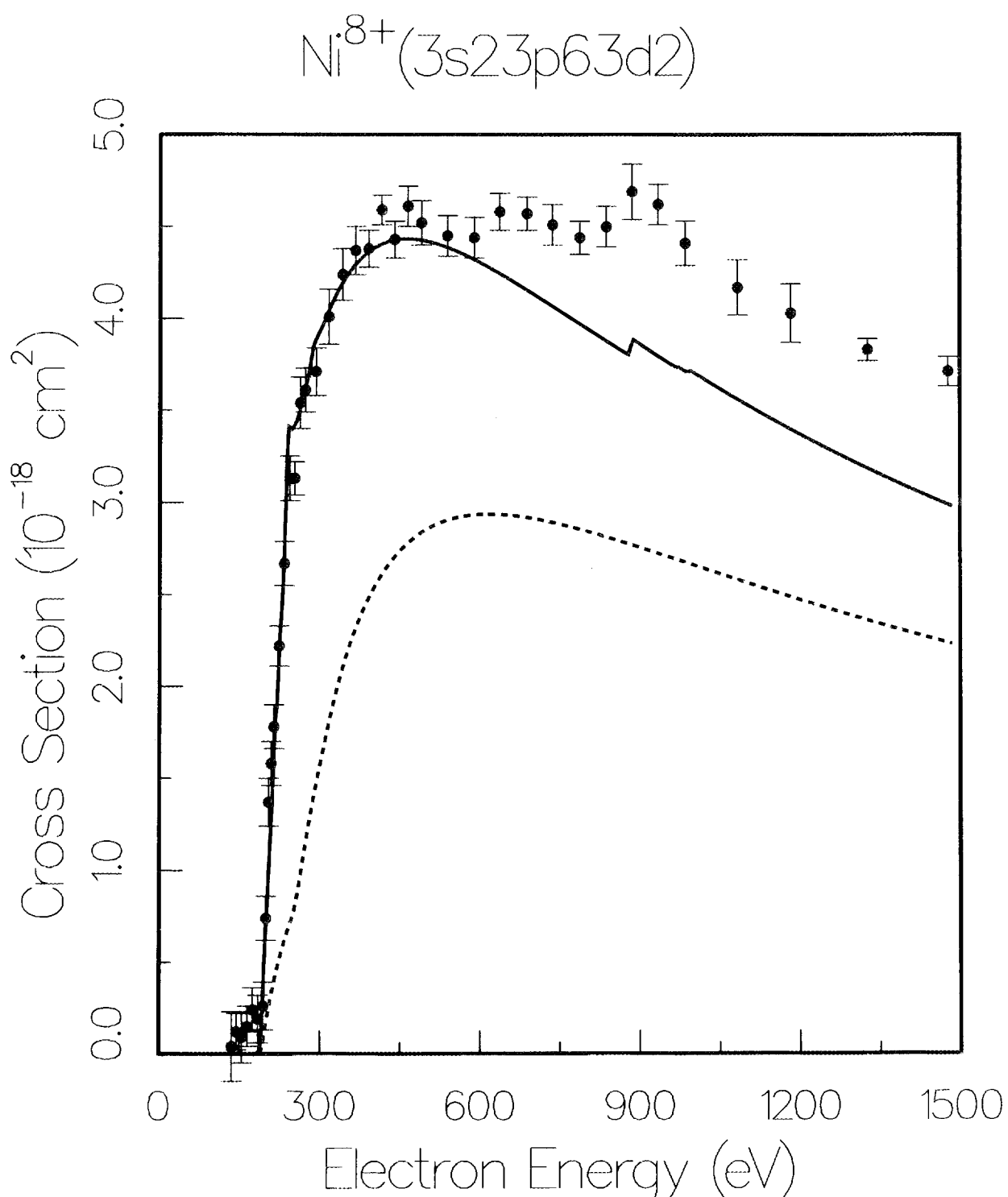


Fig. 10. Electron-impact ionization of Ni^{8+} . Full curve, configuration-average total ionization cross section from the $3d^2$ ground configuration; dashed curve, direct ionization cross section only; experimental points (ref. 15).

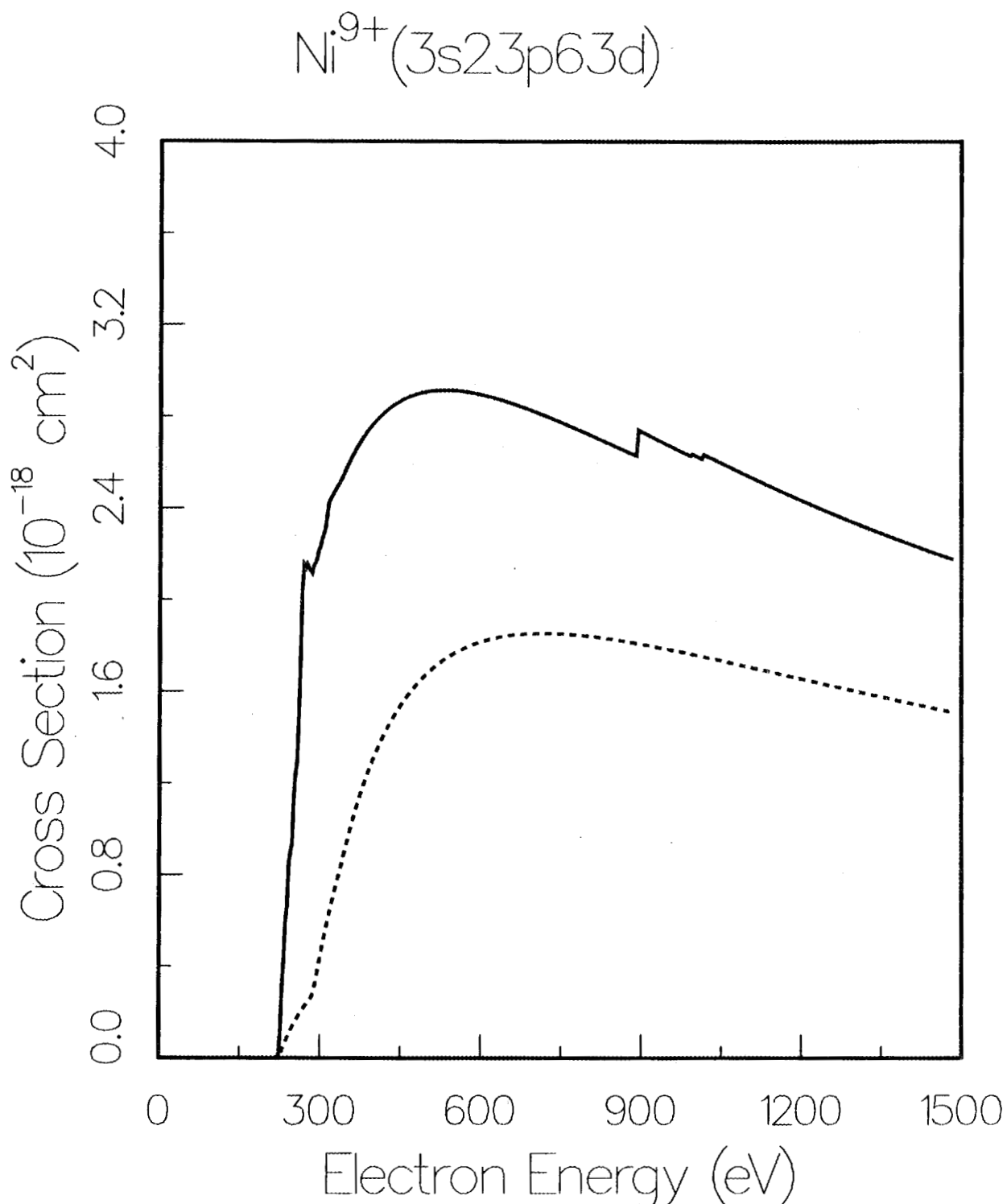


Fig. 11. Electron-impact ionization of Ni^{9+} . Full curve, configuration-average total ionization cross section from the 3d ground configuration; dashed curve, direct ionization cross section only.

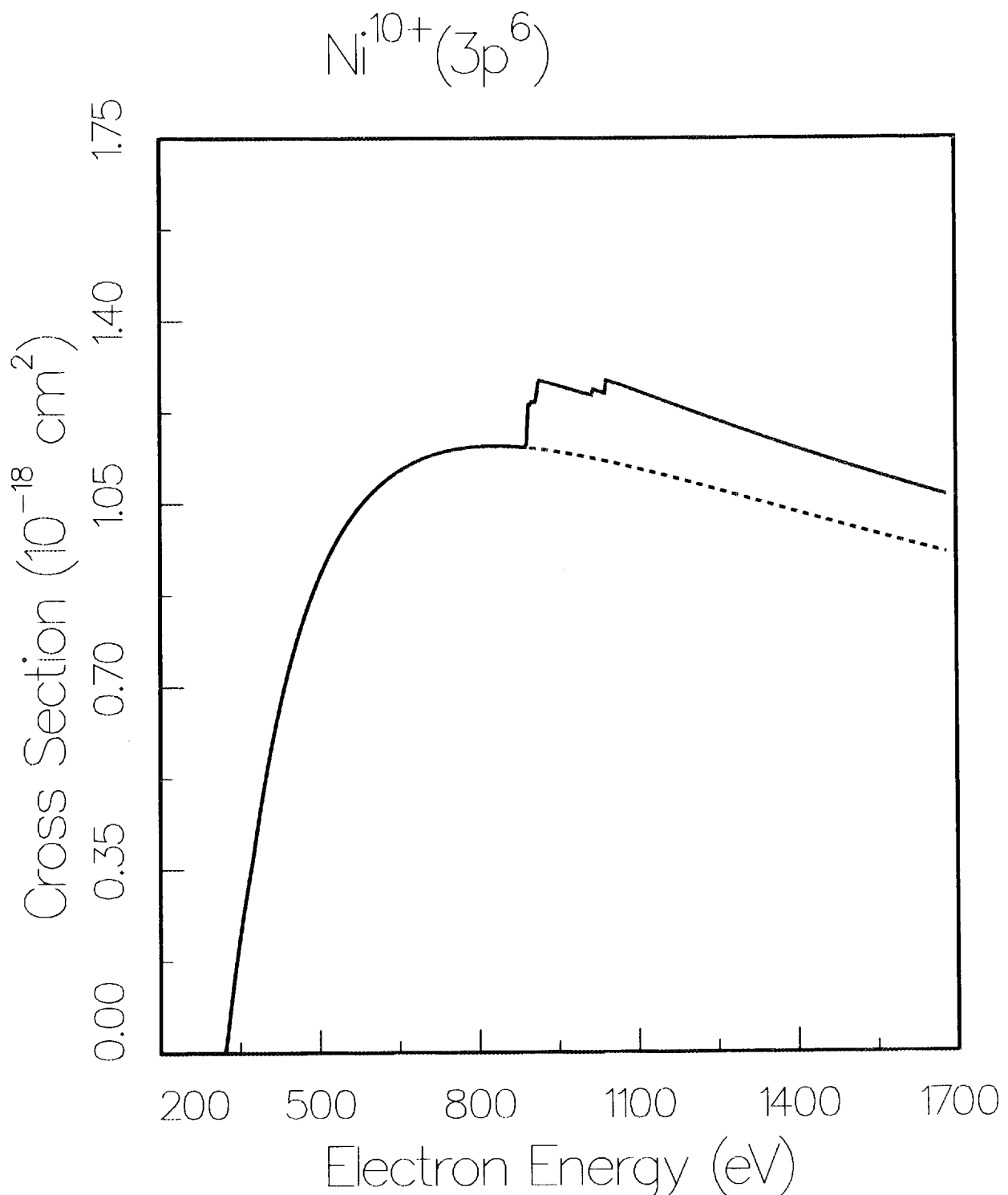


Fig. 12. Electron-impact ionization of Ni^{10+} . Full curve, configuration-average total ionization cross section from the $3p^6$ ground configuration; dashed curve, direct ionization cross section only.

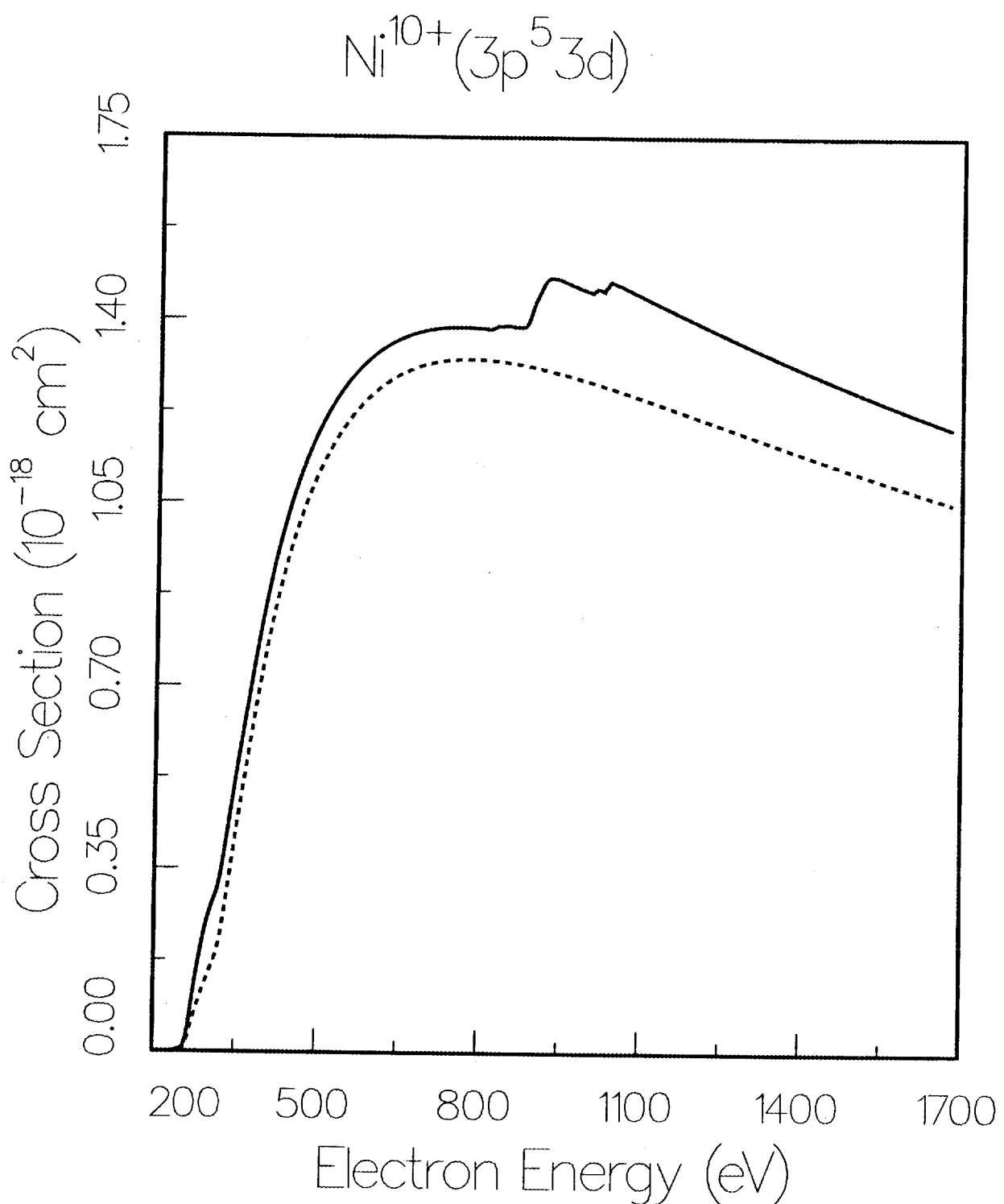


Fig. 13. Electron-impact ionization of Ni^{10+} . Full curve, configuration-average total ionization cross section from the $3p^53d$ excited configuration; dashed curve, direct ionization cross section only.

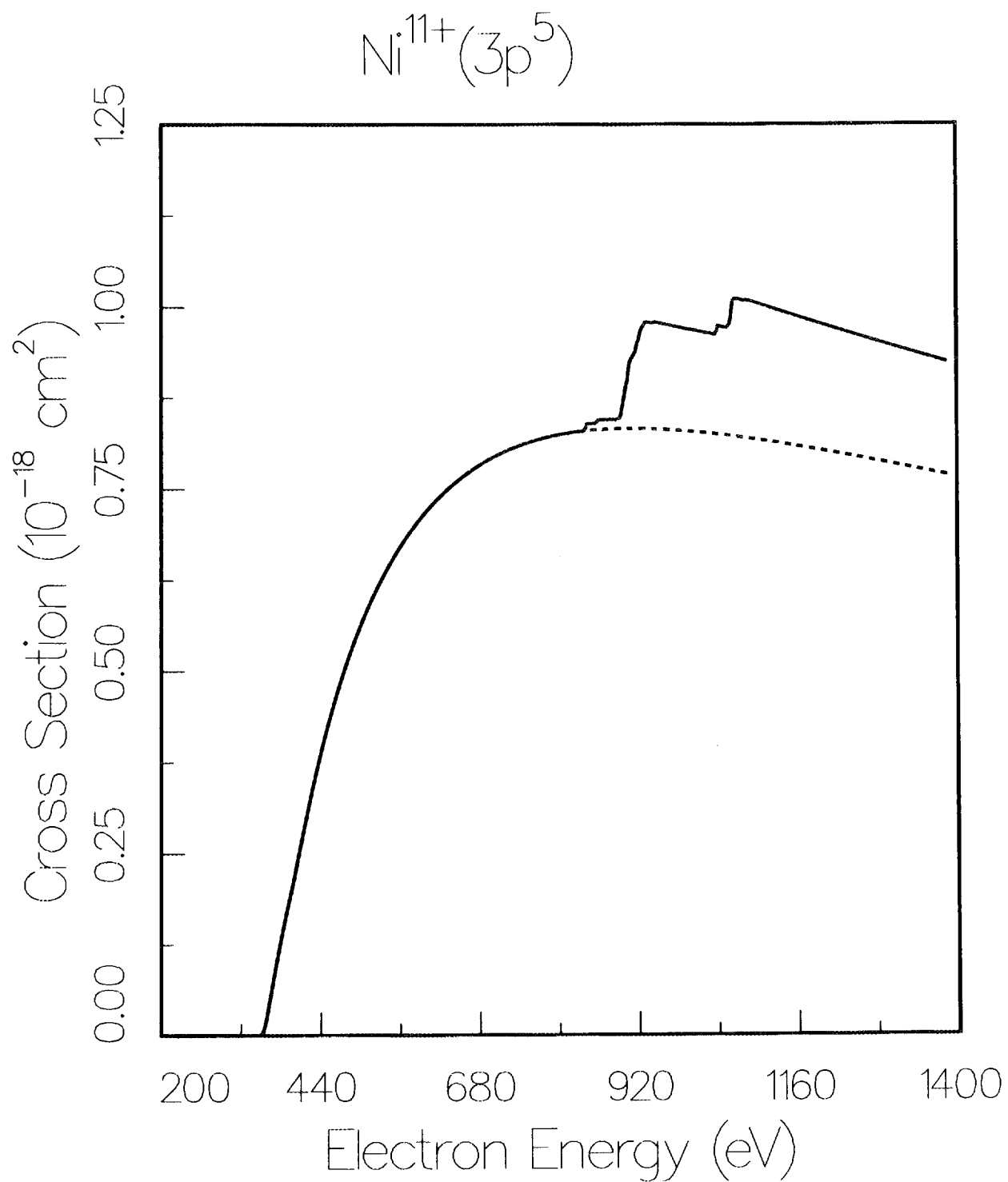


Fig. 14. Electron-impact ionization of Ni^{11+} . Full curve, configuration-average total ionization cross section from the $3p^5$ ground configuration; dashed curve, direct ionization cross section only.

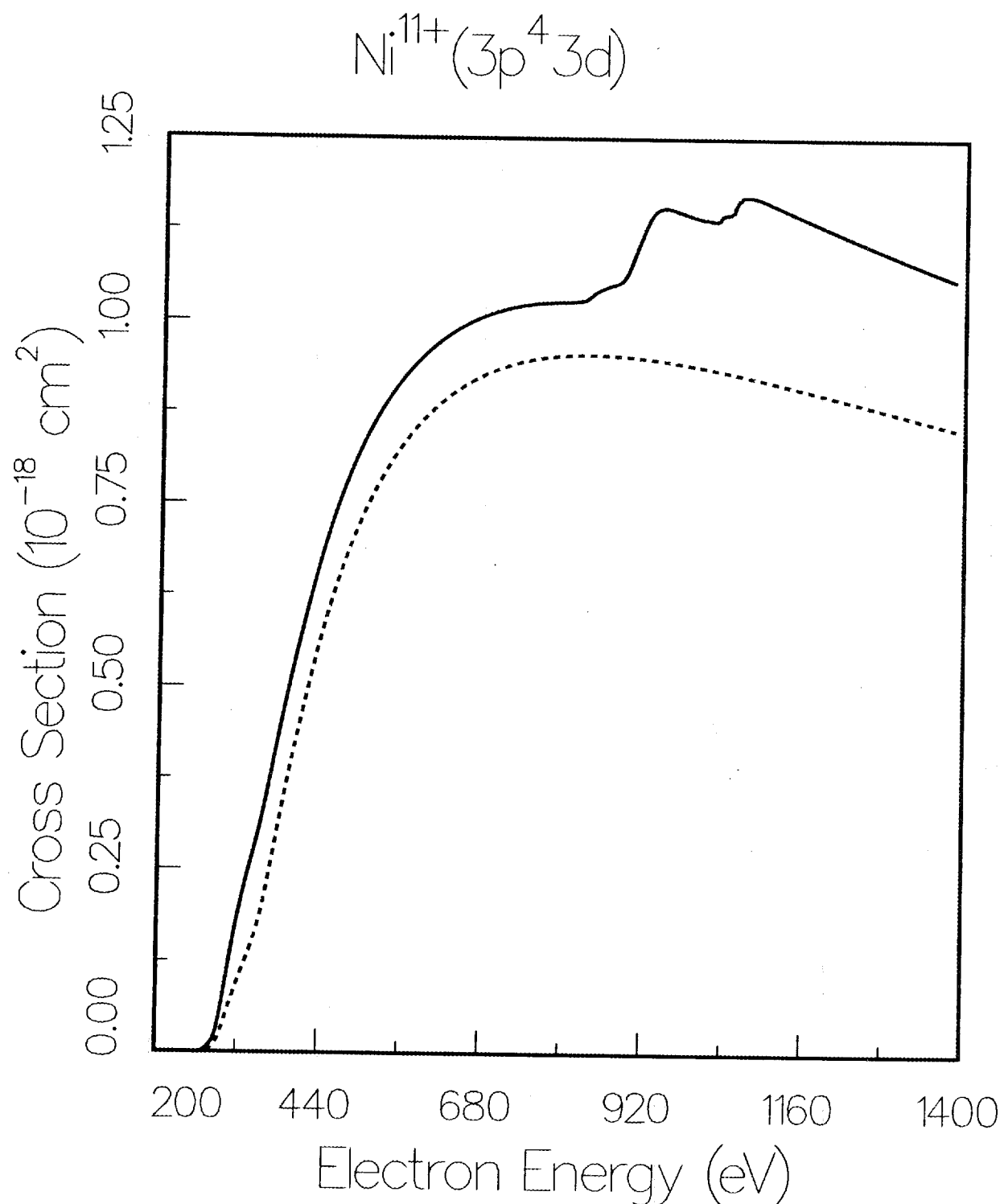


Fig. 15. Electron-impact ionization of Ni^{11+} . Full curve, configuration-average total ionization cross section from the $3p^4 3d$ excited configuration; dashed curve, direct ionization cross section only.

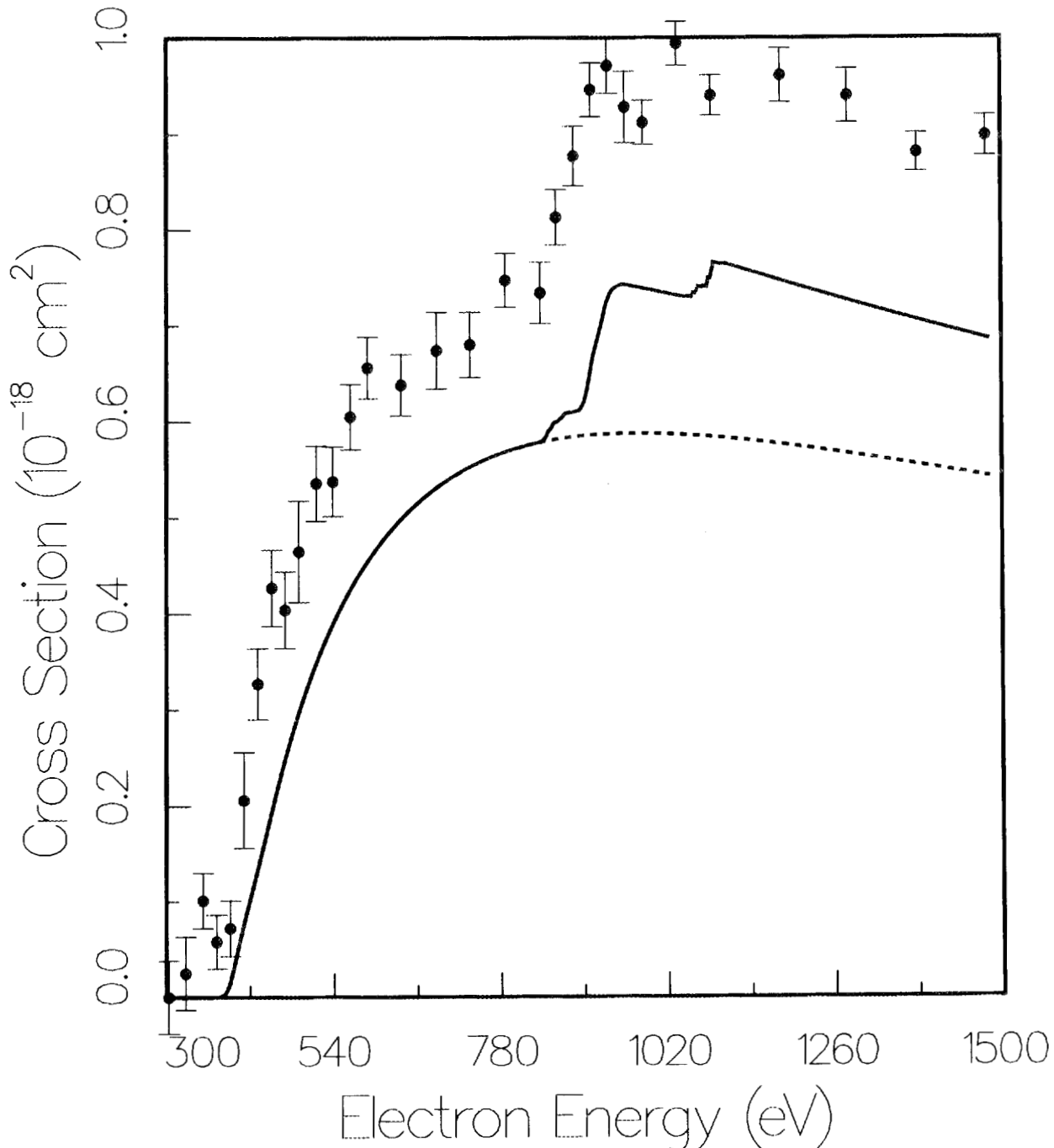
$\text{Ni}^{12+}(3p^4)$


Fig. 16. Electron-impact ionization of Ni^{12+} . Full curve, configuration-average total ionization cross section from the $3p^4$ ground configuration; dashed curve, direct ionization cross section only; experimental points (ref. 15).

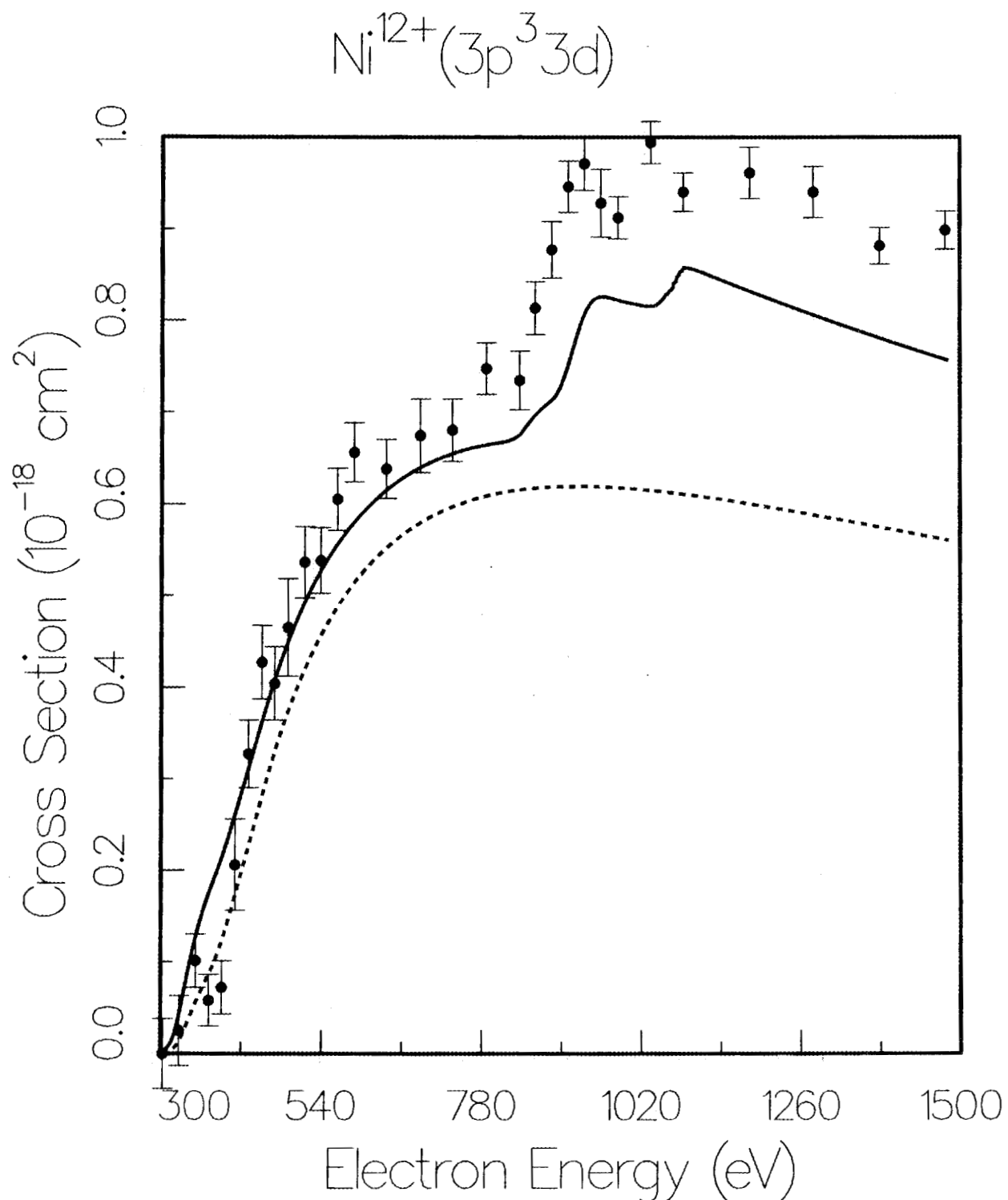


Fig. 17. Electron-impact ionization of Ni^{12+} . Full curve, configuration-average total ionization cross section from the $3p^3 3d$ excited configuration; dashed curve, direct ionization cross section only; experimental points (ref. 15).

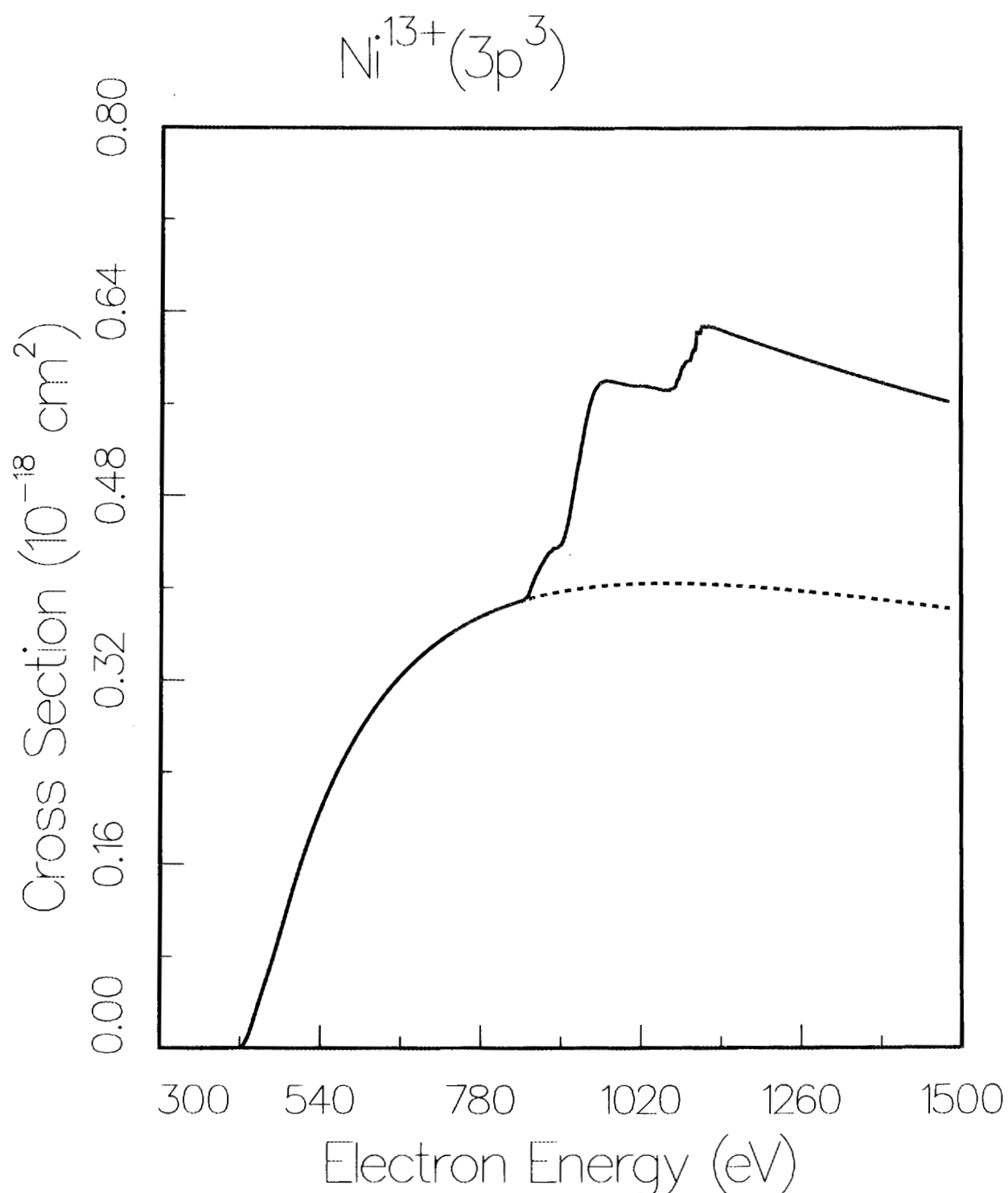


Fig. 18. Electron-impact ionization of Ni^{13+} . Full curve, configuration-average total ionization cross section from the $3p^3$ ground configuration; dashed curve, direct ionization cross section only.

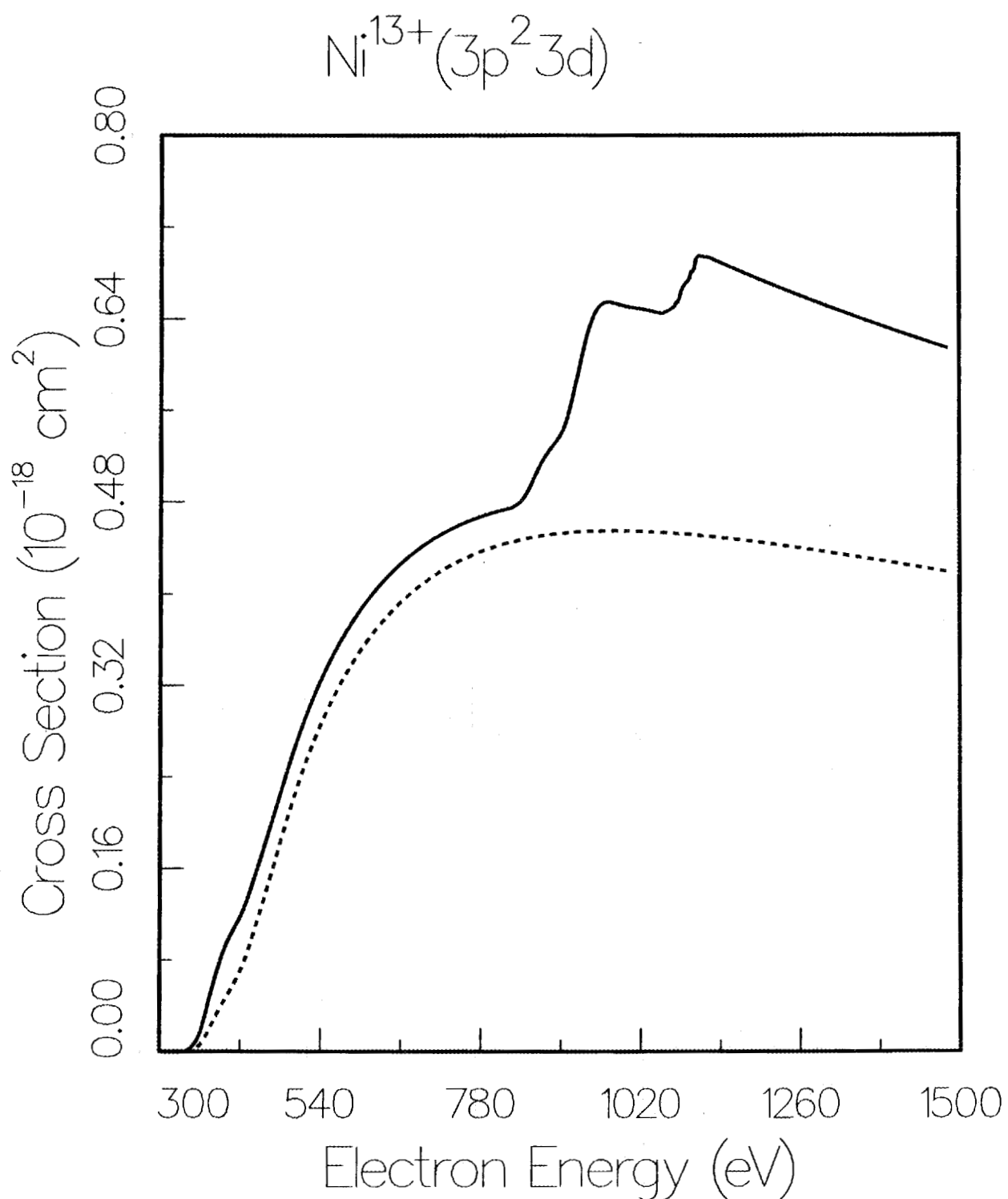


Fig. 19. Electron-impact ionization of Ni^{13+} . Full curve, configuration-average total ionization cross section from the $3p^23d$ excited configuration; dashed curve, direct ionization cross section only.

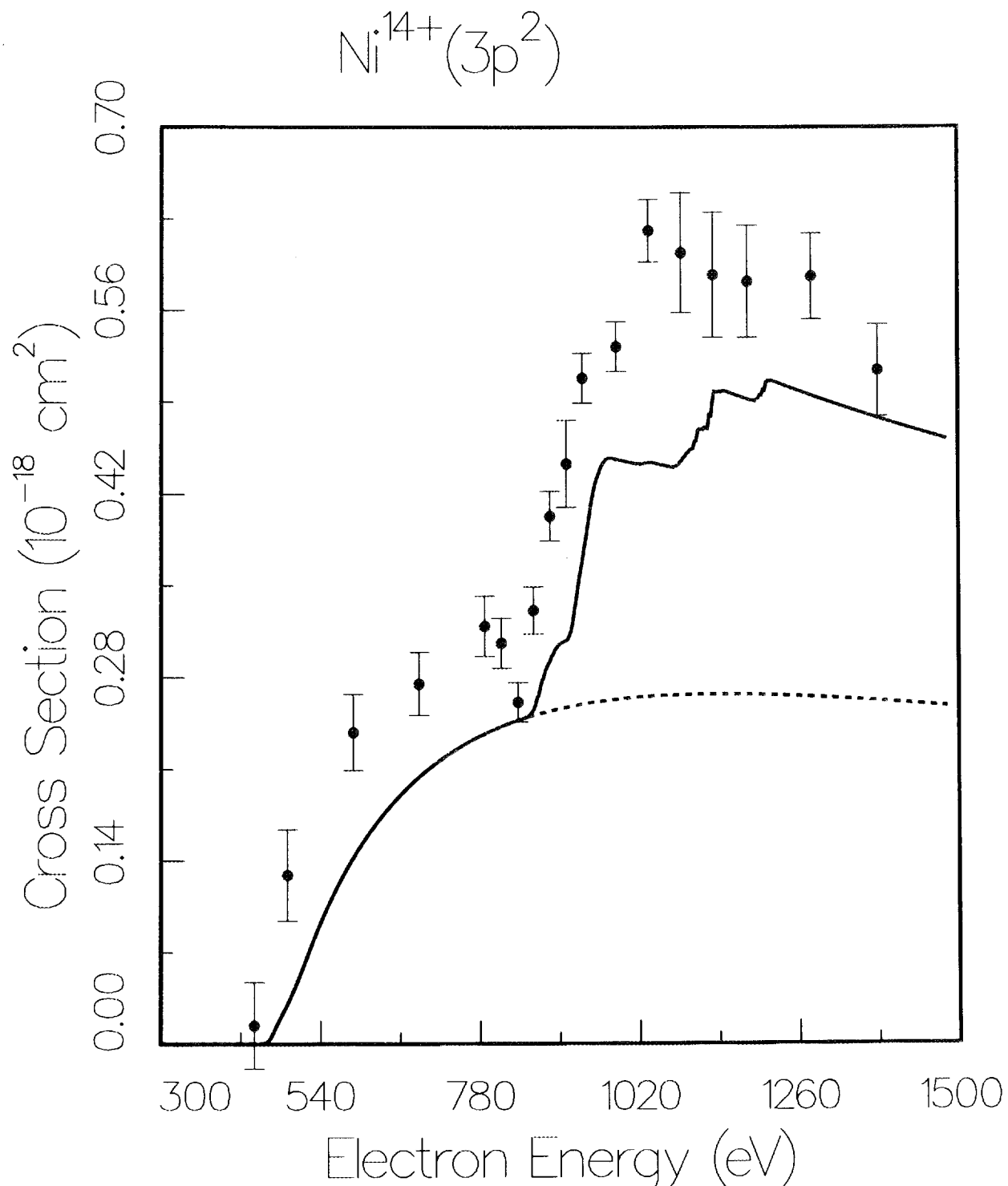


Fig. 20. Electron-impact ionization of Ni^{14+} . Full curve, configuration-average total ionization cross section from the $3p^2$ ground configuration; dashed curve, direct ionization cross section only; experimental points (ref. 15).

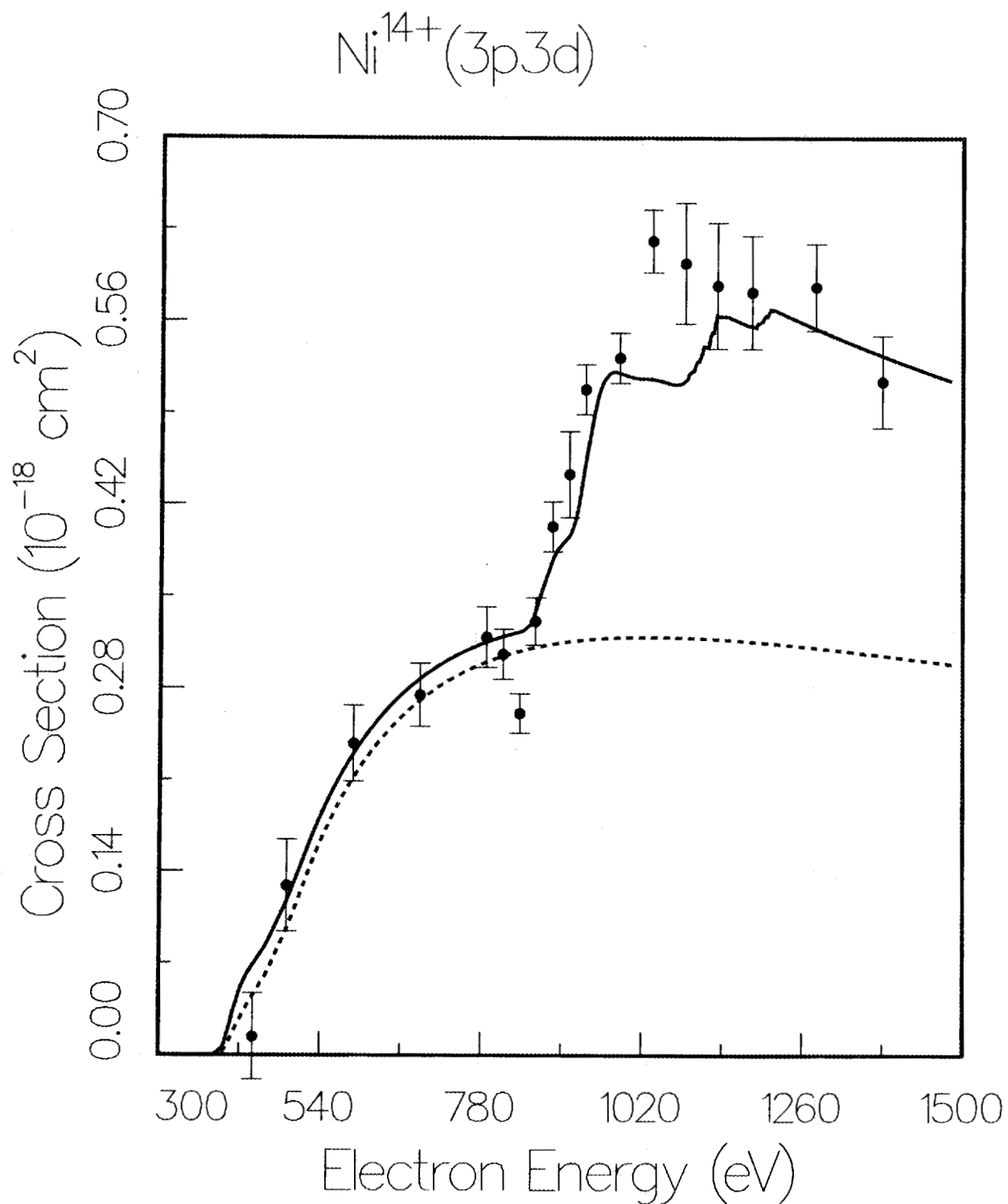


Fig. 21. Electron-impact ionization of Ni^{14+} . Full curve, configuration-average total ionization cross section from the $3\text{p}3\text{d}$ excited configuration; dashed curve, direct ionization cross section only; experimental points (ref. 15).

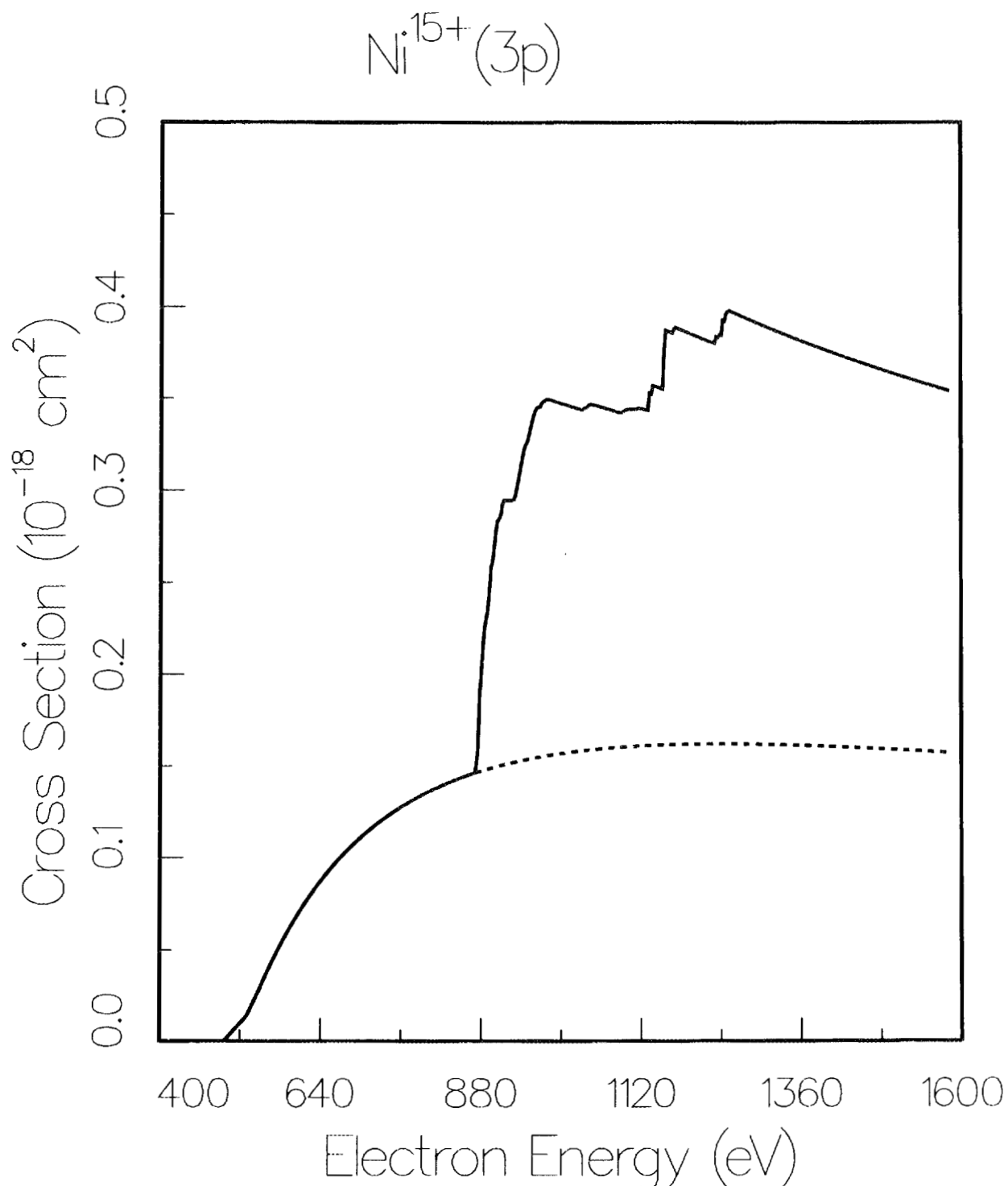


Fig. 22. Electron-impact ionization of Ni^{15+} . Full curve, configuration-average total ionization cross section from the 3p ground configuration; dashed curve, direct ionization cross section only.

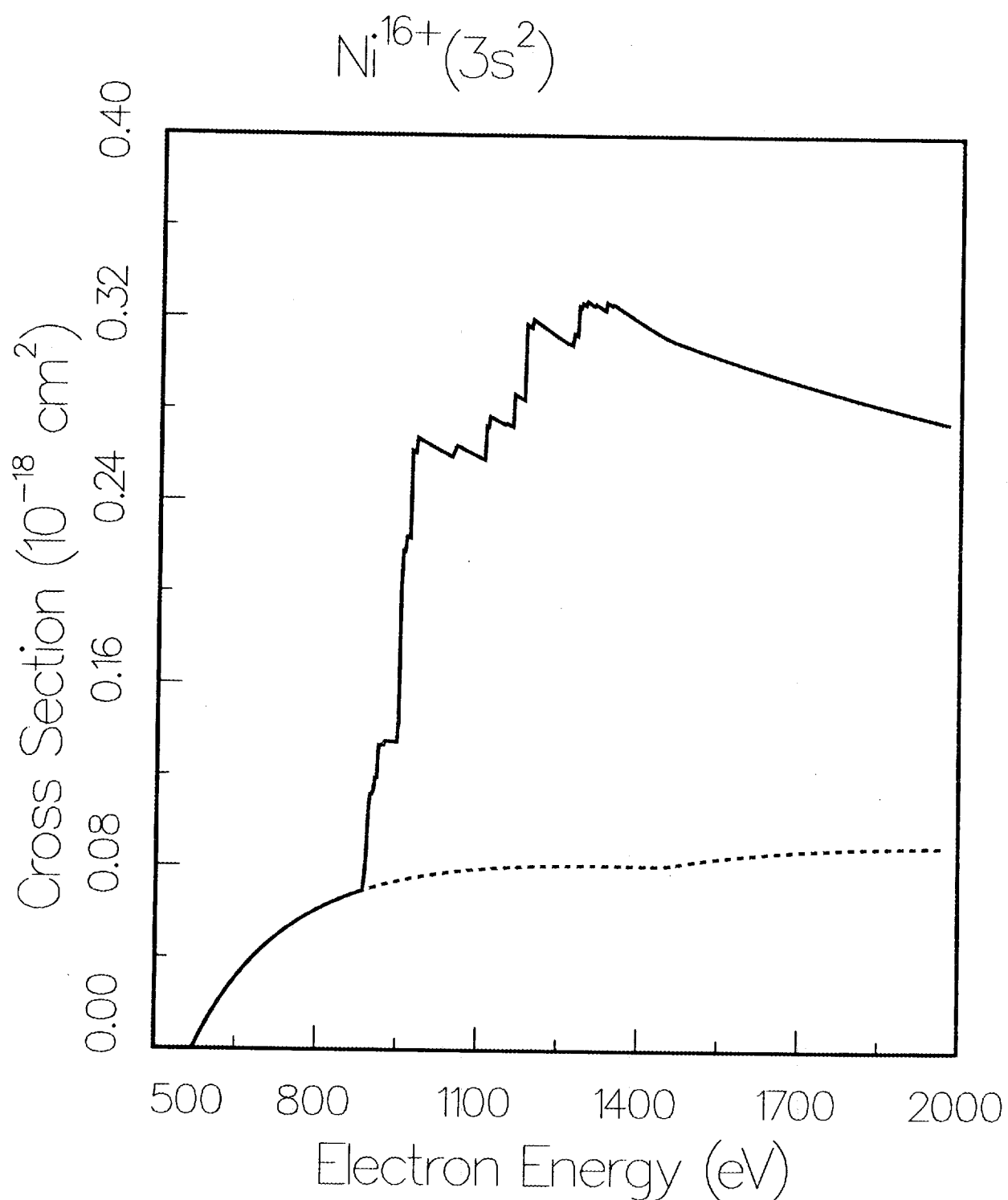


Fig. 23. Electron-impact ionization of Ni^{16+} . Full curve, level-to-level and configuration-average total ionization cross section from the $3s^2$ ground configuration; dashed curve, direct ionization cross section only.

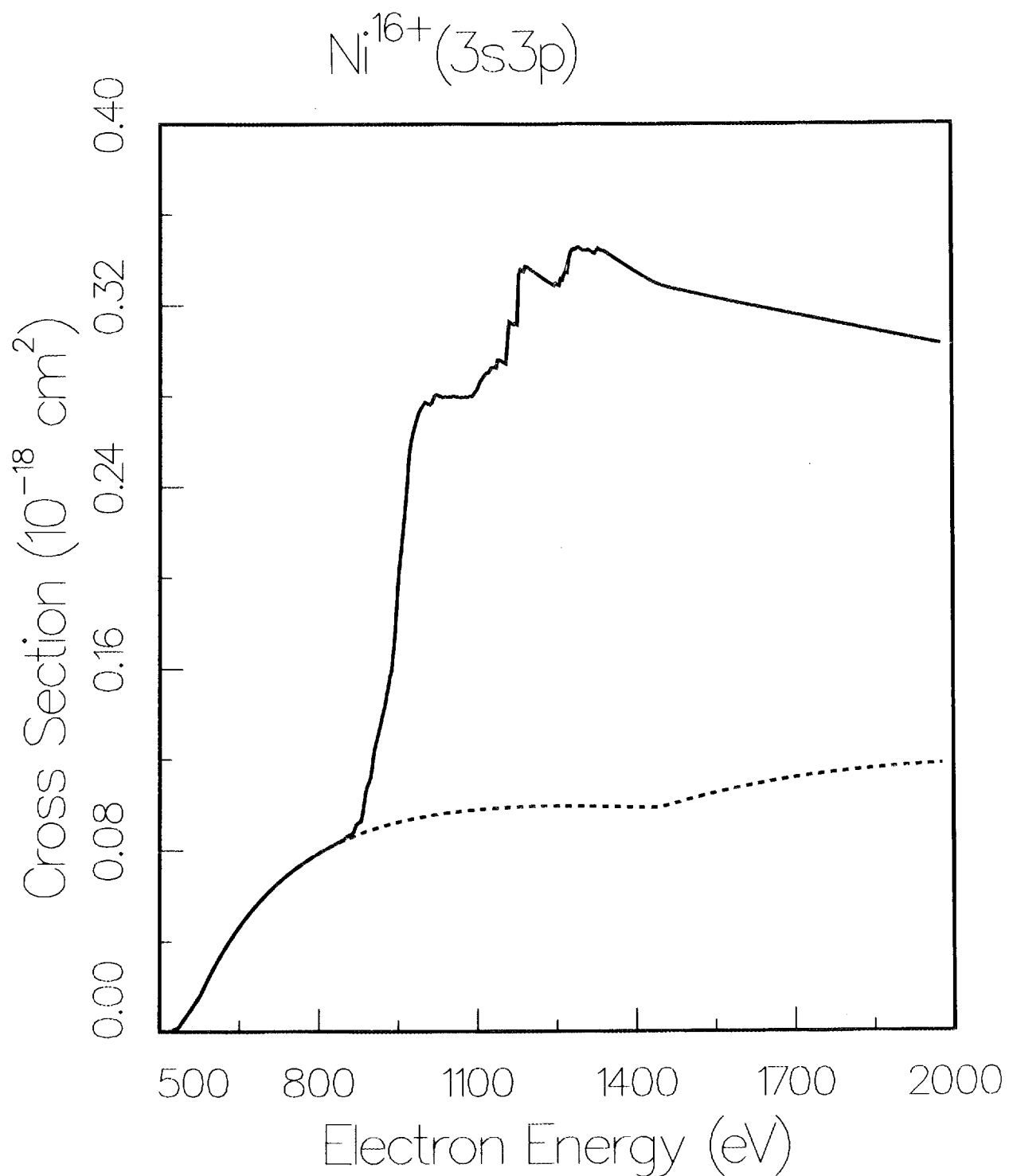


Fig. 24. Electron-impact ionization of Ni^{16+} . Full curve, level-to-level and configuration-average total ionization cross section from the $3s3p$ excited configuration; dashed curve, direct ionization cross section only.

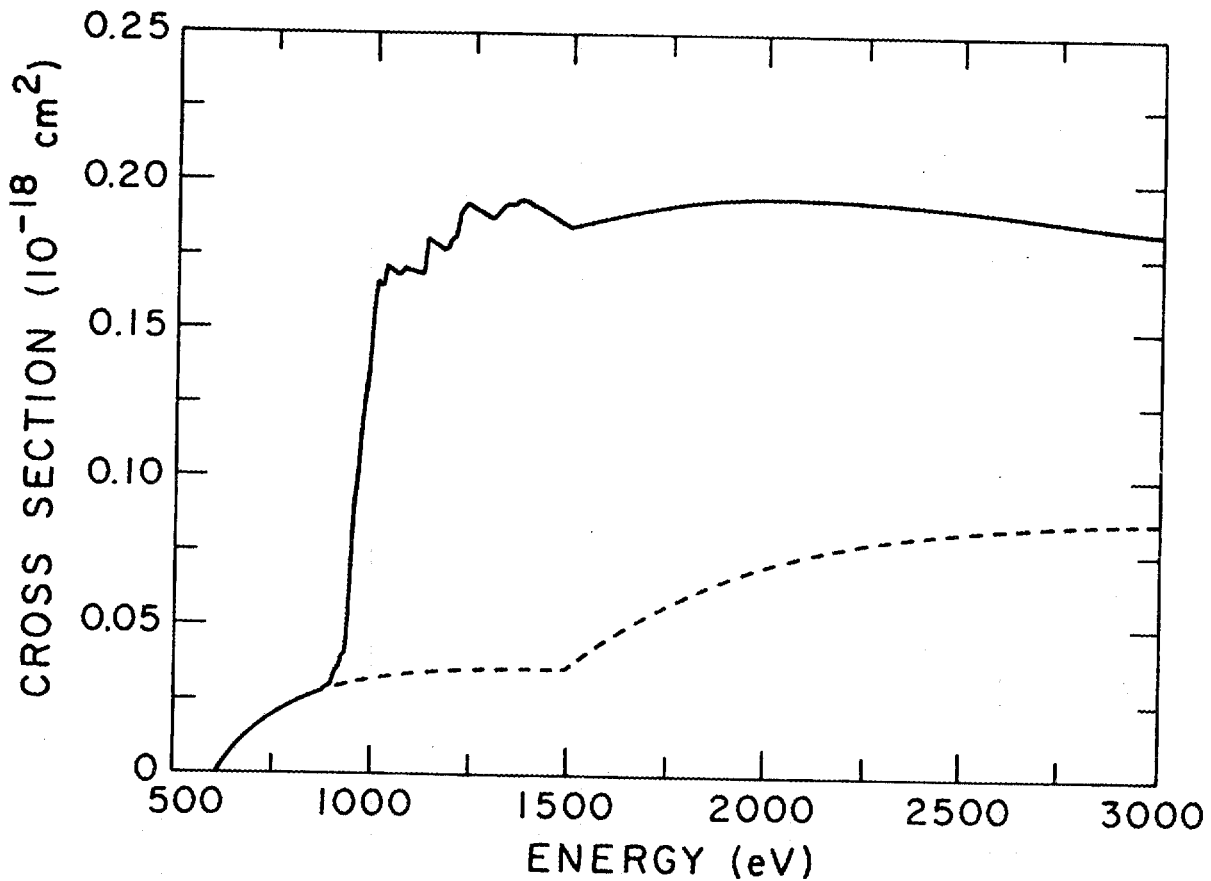


Fig. 25. Electron-impact ionization of Ni^{17+} . Full curve, level-to-level total ionization cross section from the 3s ground configuration; dashed curve, direct ionization cross section only.

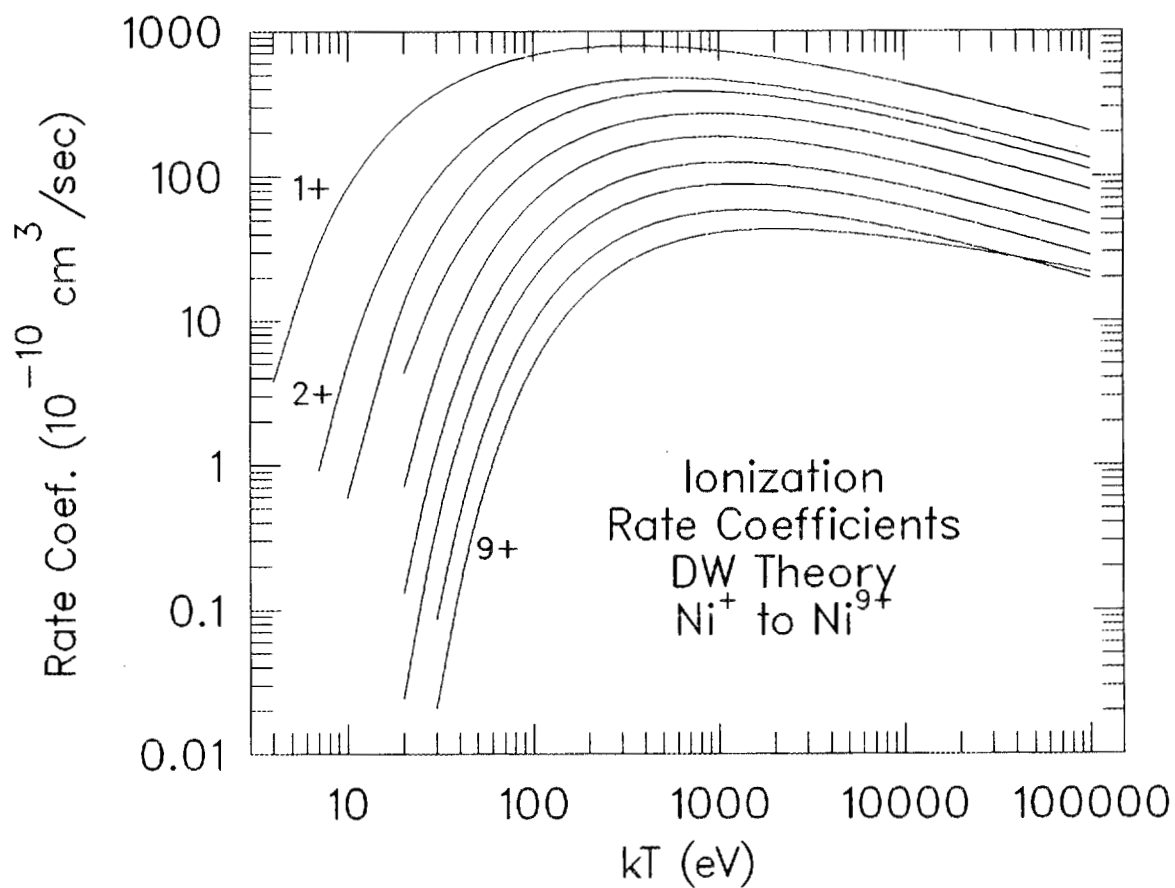


Fig. 26. Theoretical rate coefficients for Ni⁺ through Ni⁹⁺ in ground configuration.

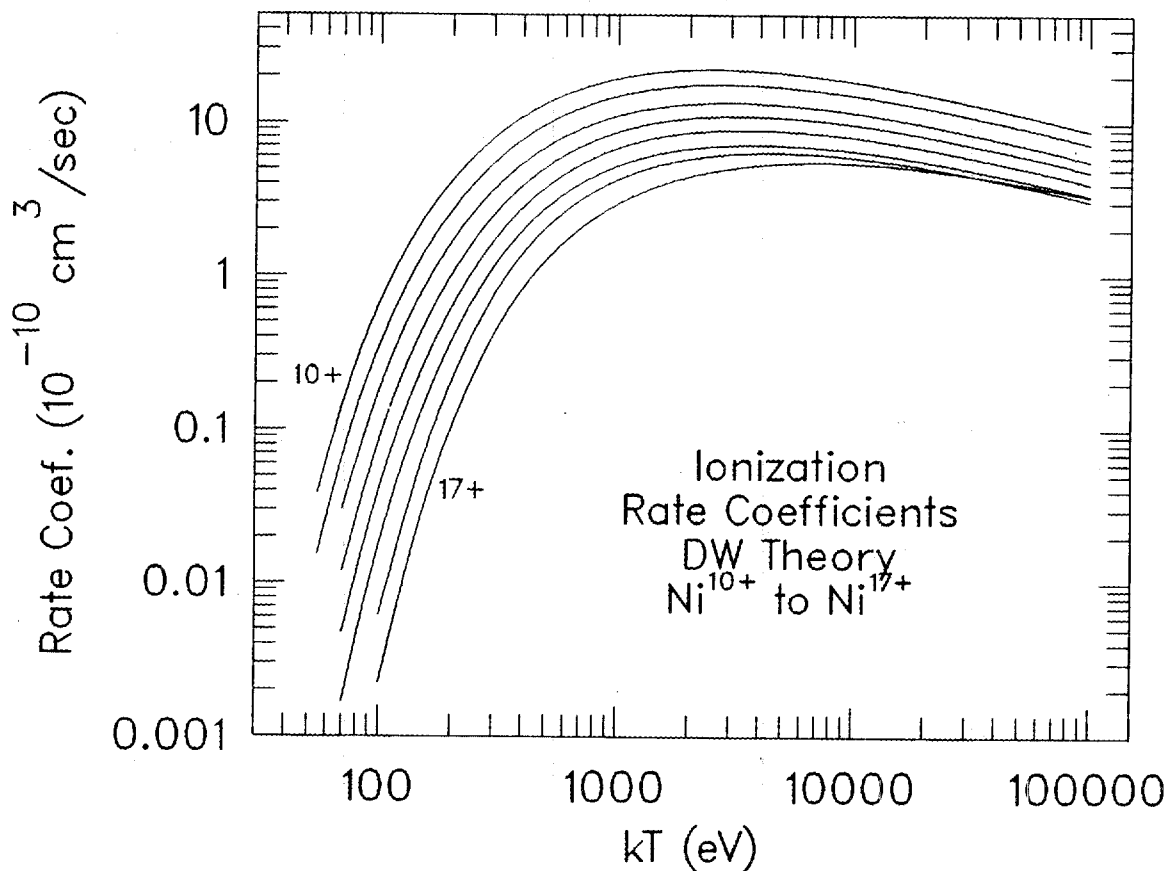


Fig. 27. Theoretical rate coefficients for Ni¹⁰⁺ through Ni¹⁷⁺ in ground configuration.

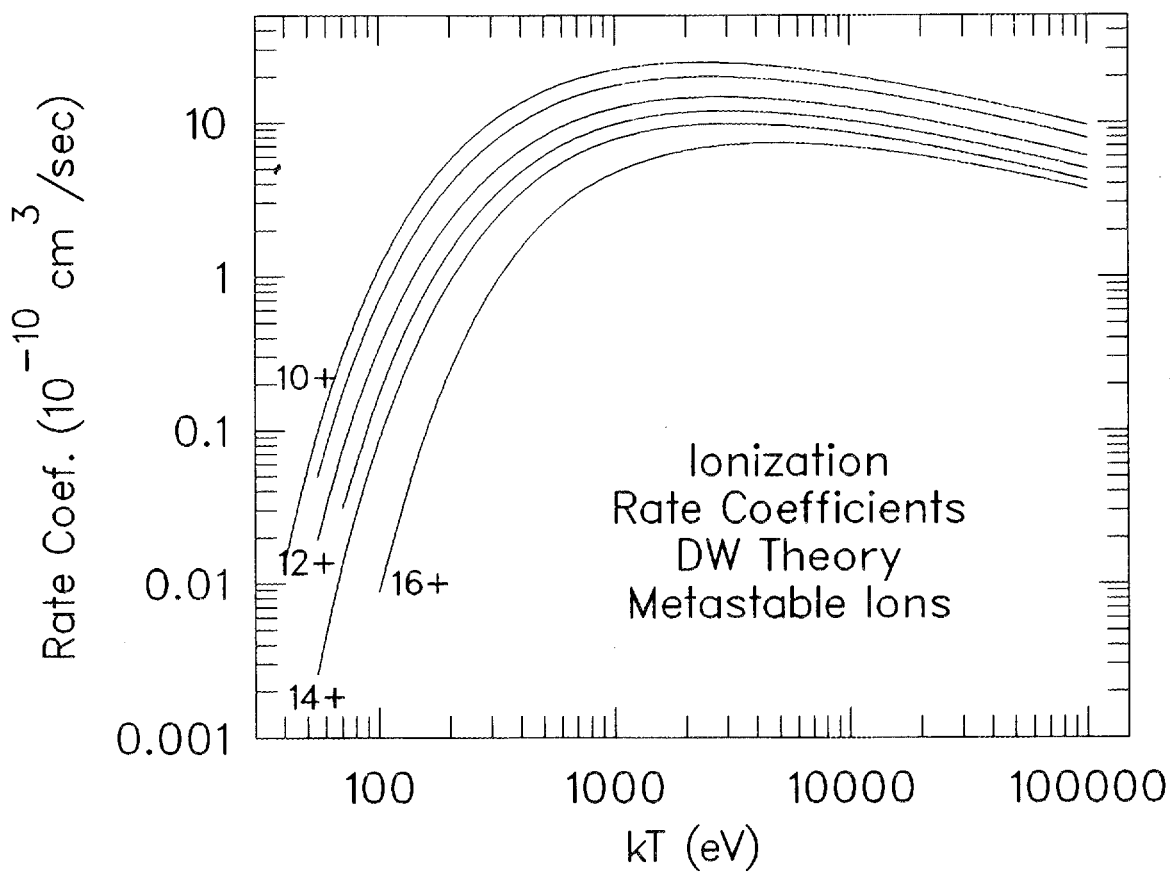


Fig. 28. Theoretical rate coefficients for Ni^{10+} through Ni^{14+} and Ni^{16+} in excited configuration.

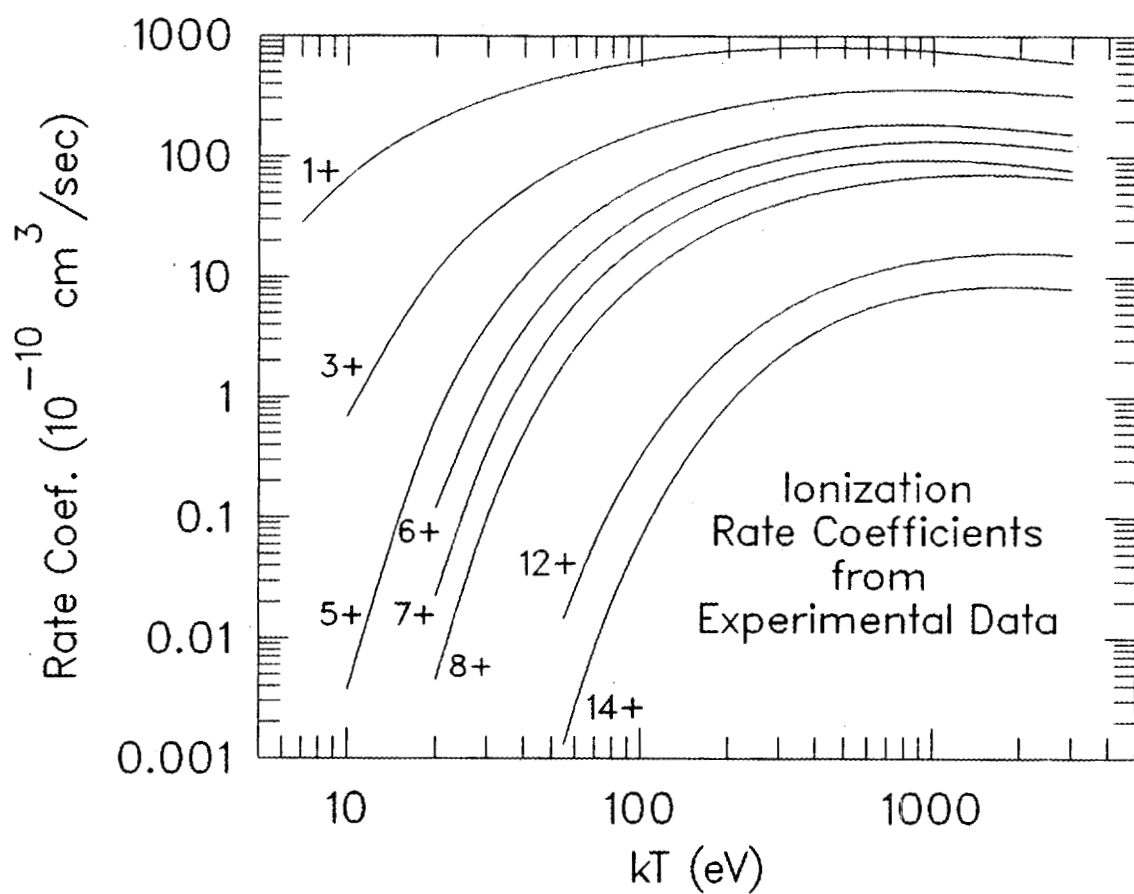


Fig. 29. Experimental rate coefficients for various Ni ions.

INTERNAL DISTRIBUTION

- | | |
|---------------------|---|
| 1. G. D. Alton | 24. R. A. Phaneuf |
| 2. R. L. Becker | 25. S. Raman |
| 3-7. C. Bottcher | 26. R. K. Richards |
| 8. E. C. Crume | 27. M. Saltmarsh |
| 9. S. Datz | 28. J. Sheffield |
| 10. P. F. Dittner | 29. C. R. Vane |
| 11. W. R. Garrett | 30-31. Controlled Fusion Atomic Data Center |
| 12. D. C. Gregory | 32. Central Research Library |
| 13. C. C. Havener | 33. Document Reference Section |
| 14. J. T. Hogan | 34-35. Laboratory Records |
| 15-19. H. T. Hunter | 36. Laboratory Records, RC |
| 20. R. C. Isler | 37. ORNL Patent Section |
| 21. C. C. Klepper | 38. Fusion Energy Div. Library |
| 22. H. F. Krause | 39. Fusion Engineering Design Center |
| 23. F. W. Meyer | |

EXTERNAL DISTRIBUTION

40. Office of the Assistant Manager for Energy Research and Development, Department of Energy, Oak Ridge Operations, Box 2001, Oak Ridge, TN 37831
41. V. A. Abramov, Institute Atommoi Energii, IV Kurchatova, 46 Ulitsa Kurchatova, Moscow D-182, U.S.S.R.
42. V. V. Afrosimov, AF Ioffe Physical-Technical Institute, Leningrad K-21 U.S.S.R. 194021
43. G. Alber, JILA, University of Colorado, Boulder, CO 80309
44. M. Ya. Amusia, AF Ioffe Physico-Technical Institute, Leningrad, U.S.S.R. 194021
45. R. Becker, Institut fuer Angewandte Physik, Universitaet Frankfurt, D-6000 Frankfurt/M, Rob.-Mayer Str. 2-4, West Germany
46. Bibliothek, Institut fuer Plasmaphysik, KFA, Postfach 1913, D-5170 Julich, Federal Republic of Germany
47. Bibliothek, Max-Planck Institut fuer Plasmaphysik, D-8046 Garching bei Munchen, Federal Republic of Germany
48. Bibliotheque, Centre de Recherches en Physique des Plasmas, 21 Avenue des Bains, 1007 Lausanne, Switzerland
49. Bibliotheque, Service due Confinement des Plasma, CEA, B.P. 6, 92 Fontenay-aux-Roses (Seine), France
50. S. L. Bliman, Centre D'Etudes Nucleaires de Grenoble, 85 X Avenue des Martyrs, F-38041 Grenoble, Cedex, France
51. F. Brouillard, Institut de Physique, Chemin du Cyclotron 2, 1348 Louvain-la-Neuve, Belgium
- 52-56. M. J. Buie, Dept. of Physics, Auburn Univ., Auburn, AL 36849
57. A. Burgess, Dept. of Applied Mathematics and Theoretical Physics, Silver Street, Cambridge, CB3 9EW, England
58. P. Burke, Dept. of Applied Mathematics, Queen's Univ. of Belfast, Belfast BT7 1NN, Northern Ireland
59. J. Callaway, Dept. of Physics and Astron., Louisiana State Univ., Baton Rouge, LA 70803
60. J. D. Callen, Dept. of Nucl. Eng., Univ. of Wisconsin, Madison, WI 53706
61. S. Chantrenne, Lawrence Livermore Natl. Lab., P.O. Box 808, Livermore, CA 94550

62. M. Chen, Lawrence Livermore Natl. Lab., P.O. Box 808, Livermore, CA 94550
63. A. Chutjian, Jet Propulsion Lab., Bldg. 183, Rm. 601, California Inst. of Technology, Pasadena, CA 91103
64. C. Cisneros, Inst. de Fisica, Apartado Postal 20-364, Mexico 20, D.F.
65. W. Claeys, Univ. Catholique de Louvain, Inst. de Physique, Chemin du Cyclotron 2, B-1348, Louvain-la-Neuve, Belgium
66. C. L. Cocke, Dept. of Physics, Kansas State Univ., Manhattan, KS 66506
67. L. A. Collins, T-4 MS-212, Los Alamos Scientific Lab., Los Alamos, NM 87545
68. R. W. Conn, Dept. of Chemical, Nuclear, and Thermal Engineering, Univ. of California, Los Angeles, CA 90024
69. R. D. Cowan, T-Division, MS 212, Los Alamos Scientific Laboratory, P.O. Box 1663, Los Alamos, NM 87544
70. D. H. Crandall, ER-54 G-219/GTN, Office of Fusion Energy, U.S. Dept. of Energy, Washington, DC 20545
71. H. E. Dalhed, L18, Lawrence Livermore Natl. Lab., P.O. Box 808, Livermore, CA 94550
72. S. O. Dean, Fusion Energy Development, Science Applications, Inc., 2 Professional Dr., Gaithersburg, MD 20760
73. P. Defrance, Univ. of Louvain, Institut de Physique, B-1348 Louvain-la-Neuve, Belgium
74. F. J. De Heer, FOM-Inst. of Atomic and Molecular Physics, Kruislaan 407, Amsterdam/Watergraafsmeer, The Netherlands
75. Documentation S.I.G.N., Dept. de la Physique du Plasma et de la Fusion Controlee, Centre d'Etudes Nucleaires, B.P. No. 85, Centre du Tri, 38041 Cedex, Grenoble, France
76. K. T. Dolder, Dept. of Atomic Physics, The University, Newcastle Upon Tyne, England, NE17RU
77. Bob DuBois, Battelle Northwest, Battelle Blvd., Richland, WA 99352
78. J. Duggan, Dept. of Physics, North Texas State Univ., Denton, TX 76203
79. G. H. Dunn, JILA, Univ. of Colorado, Campus Box 440, Boulder, CO 80309-0440
80. H. Ehrhardt, Fachbereich Physik, Universitaet Keiserlautern, D-6750 Kaiserlautern, West Germany
81. G. A. Eliseev, I. V. Kurchatov Inst. of Atomic Energy, P.O. Box 3402, 123182 Moscow, U.S.S.R.
82. R. A. Falk, Boeing Aerospace Co., P.O. Box 3999, MS 87-50, Seattle, WA 98124
83. U. Fano, James Franck Inst., Rm. 227, Univ. of Chicago, 5430 Ellis Ave., Chicago, IL 60637
84. J. L. Feldman, Cond. Matter Phys. Branch, Code 6683, U.S. Naval Research Lab., Washington, DC 20375
85. C. F. Fischer, Dept. of Computer Science, P.O. Box 6035, Station B, Vanderbilt Univ., Nashville, TN 37235
86. H. K. Forsen, Bechtel Group, Inc., Research Engineering, P.O. Box 3965, San Francisco, CA 94105
87. T. F. Gallagher, Physics Dept., Univ. of Virginia, Charlottesville, VA 22901
88. S. Geltman, JILA, Univ. of Colorado, Boulder, CO 80309
89. H. B. Gilbody, Dept. of Pure and Applied Physics, The Queen's Univ. of Belfast, Belfast BT7 1NN, Northern Ireland
90. J. R. Gilleland, GA Technologies, Inc., Fusion and Advanced Technology, P.O. Box 85608, San Diego, CA 92138
91. V. A. Glukhikh, Scientific-Research Inst. of Electro-Physical Apparatus, 188631 Leningrad, U.S.S.R.
92. L. B. Golden, Dept. of Physics, Worthington Scranton Campus, Pennsylvania State Univ., 120 Ridge View Dr., Dunmore, PA 18512
93. R. W. Gould, Dept. of Applied Physics, California Inst. of Technology, Pasadena, CA 91125
- 94-98. D. C. Griffin, Physics Dept., Rollins College, Winter Park, FL 32789

99. I. W. Griffiths, Royal Society Research Unit, Univ. College of Swansea, Singleton Park, Swansea, United Kingdom
100. R. A. Gross, Plasma Research Lab., Columbia Univ., New York, NY 10027
101. Y. Hahn, Dept. of Physics, Univ. of Connecticut, Storrs, CT 06268
102. M.F.A. Harrison, Culham Lab., Rm. 131/F7, UKAEA Research Group, Abingdon, Oxfordshire, OX 14 3DB, England
103. A. U. Hazi, Lawrence Livermore Natl. Lab., P.O. Box 808, Livermore, CA 94550
104. R.J.W. Henry, Dept. of Physics and Astronomy, Louisiana State Univ., Baton Rouge, LA 70803
105. A. P. Hickman, Molecular Physics Lab., SRI International, Menlo Park, CA 94023
106. E. Hinnov, Plasma Physics Lab., Princeton Univ., Princeton, NJ 08540
107. J. Hiskes, Lawrence Livermore Natl. Lab., Livermore, CA 94550
108. J. H. Hughes, Dept. of Computer Science, Queen's Univ., Belfast, Northern Ireland
109. R. A. Hulse, Plasma Physics Lab., Princeton Univ., P.O. Box 451, Princeton, NJ 08544
110. M. Inokuti, Environmental Research Division, Argonne Natl. Lab., Argonne, IL 60439
111. Y. Itikawa, Inst. of Space & Astronautical Science, 3-1-1 Yoshinodai, Sagamiharashi 229, Japan
112. V. L. Jacobs, Plasma Physics Division, Naval Research Laboratory, Washington, DC 20375
113. R. K. Janev, IAEA, Wagramerstrasse 5, P.O. Box 100, A-1400 Vienna, Austria
114. C. J. Joachain, Institut de Physique, Sciences 1, Univ. de Louvain, B1348 Louvain-la-Neuve, Belgium
115. Joint Institute for Laboratory Astrophysics, Publications Distribution Center, Univ. of Colorado, Boulder, CO 80309
116. K. W. Jones, Brookhaven Natl. Lab., Upton, NY 11973
117. E. Kallne, JET Joint Undertaking, Abingdon, Oxon OX14 3EA England
118. Y. Kaneko, Tokyo Metropolitan Univ., Ketagaya-ku, Tokyo, 158, Japan
119. T. Kato, Inst. of Plasma Physics, Nagoya Univ., Nagoya 464, Japan
120. H. P. Kelly, Dept. of Physics, Univ. of Virginia, Charlottesville, VA 22901
121. Y-K. Kim, National Institute of Standards and Technology, A261, Phys. Bldg., Gaithersburg, MD 20899
122. A. E. Kingston, Dept. of Applied Mathematics, Queen's Univ. of Belfast, Belfast BT7 1NN, Northern Ireland
123. M. Klapisch, Physics Dept., Racah Inst., Hebrew Univ., Jerusalem, Israel
124. J. L. Kohl, Center for Astrophysics, 60 Garden St., Cambridge, MA 02138
125. K. LaGattuta, Physics Dept., Univ. of Connecticut, Storrs, CT 06268
126. Y. T. Lee, Lawrence Livermore Natl. Lab., L-355, P.O. Box 808, Livermore, CA 94550
127. Library, Culham Lab., UKAEA, Abingdon, Oxfordshire, OX14 3DB, England
128. Library, ROM Inst. voor Plasma-Fysica, Rijnhuizen, Jutphaas, The Netherlands
129. Library, Inst. of Physics, Academia Sinica, Beijing, People's Republic of China
130. Library, National Inst. of Fusion Science, Nagoya Univ., Nagoya 464, Japan
131. Library, International Center for Theoretical Physics, Trieste, Italy
132. Library, Laboratorio Gas Ionizzati, Frascati, Italy
133. Library, Plasma Physics Laboratory, Kyoto Univ., Gokasho Uji, Kyoto, Japan
134. A. Lorenz, IAEA, Wagramerstrasse 5, P.O. Box 100, A-1400 Vienna, Austria
135. J. B. Mann, Los Alamos National Lab., P.O. Box 1663, Los Alamos, NM 86544
136. M.R.C. McDowell, Dept. of Mathematics, Royal Holloway College, Egham, Surrey TW20 OEX, England
137. E. J. McGuire, Sandia Labs, Orgn. 1231, Albuquerque, NM 87115
138. D. M. Meade, Plasma Physics Lab., Princeton Univ., P.O. Box 451, Princeton, NJ 08544
139. W. Mehlhorn, Fakultaet fuer Physik, Universitaet Freiburg, D-78 Freiburg, Federal Republic of Germany
140. A. L. Merts, T-4, MS 212, Los Alamos Natl. Lab., Los Alamos, NM 87544

141. D. R. Mikkelsen, Plasma Physics Lab., P.O. Box 451, Princeton, NJ 08544
142. J.B.A. Mitchell, Physics Dept., Univ. Western Ontario, London, Ontario, Canada N6A5B9
143. D. L. Moores, Dept. of Physics and Astronomy, Univ. College London, Gower St., London WC1E 6BT, United Kingdom
144. T. J. Morgan, Dept. of Physics, Wesleyan Univ., Middletown, CT 06457
145. W. L. Morgan, Lawrence Livermore Natl. Lab., L-18, P.O. Box 808, Livermore, CA 94550
146. R. L. Morse, Dept. of Physics, Univ. of Arizona, Tucson, AZ 85721
147. A. Msezane, Dept. of Physics, Morehouse College, 233 Chestnut St., SW, Atlanta, GA 30314
148. D. Mueller, Dept. of Physics, Univ. of North Texas, P.O. Box 5368, Denton, TX 76203
149. A. Muller, Strahlzentrum Justus Liebig Univ., Inst. fuer Kernphysik, Leihgesterner Weg 217, 6300 Giessen, West Germany
150. D. W. Norcross, JILA University of Colorado, Boulder, CO 80309
151. S. Ohtani, National Inst. of Fusion Science, Nagoya Univ., Nagoya 464, Japan
152. R. E. Olson, Physics Dept., Univ. of Missouri-Rolla, Rolla, MO 65401
153. B. Peart, Dept. of Atomic Physics, The University, Newcastle Upon Tyne, England NE1 7RU
154. J. M. Peek, Group T-4, MS-B212, Los Alamos National Lab., Los Alamos, NM 87545
- 155-
159. M. S. Pindzola, Physics Dept., Auburn Univ., Auburn, AL 36849
160. Plasma Research Laboratory, Australian National Univ., P.O. Box 4, Canberra, A.C.T. 2000, Australia
161. D. E. Post, Jr., Princeton Plasma Physics Lab., P.O. Box 451, Princeton, NJ 08544
162. A. Pradhan, JILA, Univ. of Colorado, Boulder, CO 80309
163. R. V. Pyle, Magnetic Fusion Group, Lawrence Berkeley Lab., Univ. of California, Berkeley, CA 94720
164. J. F. Reading, Physics Dept., Texas A&M Univ., College Station, TX 77840
165. P. J. Reardon, Brookhaven National Lab., Upton, NY 11973
166. J. R. Roberts, A 59-221, National Institute of Standards and Technology, B070, Phys. Bldg., Gaithersburg, MD 20899
167. L. Roszman, National Institute of Standards and Technology, A255, Physics Bldg., Gaithersburg, MD 20899
168. W. L. Rowan, Fusion Research Center, Univ. of Texas, Austin, TX 78712
169. D. D. Ryutov, Inst. of Nuclear Physics, Siberian Branch, Academy of Sciences of the U.S.S.R., Sovetskaya St. 5, 630090 Novosibirsk, U.S.S.R.
170. E. Salzborn, Strahlzentrum, Justus Liebig Univ., Inst. fuer Kernphysik, Leihgesterner Weg 217, 6300 Giessen, West Germany
171. D. H. Sampson, 505 Davey Lab., Pennsylvania State Univ., University Park, PA 16802
172. M. J. Seaton, Dept. of Physics, Univ. College London, Gower St., London WC1 6BT, England
173. A.C.H. Smith, JILA, Univ. of Colorado, Boulder, CO 80309
174. J. J. Smith, IAEA, Wagramerstrasse 5, P.O. Box 100, A-1400 Vienna, Austria
175. I. Spighel, Lcbedev Physical Inst., Leninsky Prospect 53, 117924 Moscow, U.S.S.R.
176. R. Srivastava, Dept. of Physics, Univ. of Roorkee, Roorkee 247672, India
177. W. M. Stacey, Jr., School of Nuclear Engineering, Georgia Inst. of Technology, Atlanta, GA 30332
178. D. Steiner, Rensselaer Polytechnic Inst., Troy, NY 12181
179. B. Stratton, Princeton Plasma Physics Lab., P.O. Box 451, Princeton, NJ 08544
180. H. Summers, JET Joint Undertaking, Abingdon, Oxon OX14 3EA England
181. H. Tawara, National Inst. of Fusion Science, Nagoya Univ., Nagoya 464-01, Japan

182. H. Taylor, Chemistry Dept., Univ. of Southern California, University Park, Los Angeles, CA 90007
183. A. Temkin, Atomic Physics Office, Code 680.1, Goddard Space Flight Center, Greenbelt, MD 20771
184. Thermonuclear Library, Japan Atomic Energy Research Inst., Tokai, Naka, Ibaraki, Japan
185. V. T. Tolok, Kharkov Physical-Technical Inst., Academical St. 1, 310108 Kharkov, U.S.S.R.
186. R. Varma, Physical Research Lab., Navrangpura, Ahmedabad, India
187. E. Wahlin, JILA, Univ. of Colorado, Boulder, CO 80309
188. J. F. Williams, Physics Dept., Univ. of Western Australia, Perth 6009, Australia
- 189-
198. Office of Scientific and Technical Information, P.O. Box 62, Oak Ridge, TN 37831